ELSEVIER

Contents lists available at ScienceDirect

Chemical Engineering Journal Advances

journal homepage: www.sciencedirect.com/journal/chemical-engineering-journal-advances



CFD approaches in microfluidics for the development of polymeric, lipid-based and inorganic nanoparticles for drug delivery

Anna Tsitouridou ^a, Maryam Parhizkar ^b, Chuan-Yu Wu ^a, Tao Chen ^a, Dimitrios Tsaoulidis ^{a,*} ^o

- ^a School of Chemistry and Chemical Engineering, University of Surrey, GU2 7XH, Guildford, UK
- ^b School of Pharmacy, University College London, WC1E 6BT, London, UK

ARTICLE INFO

Keywords: CFD modelling Nanoparticles Microfluidic synthesis Drug delivery system

ABSTRACT

Microfluidics is an innovative approach for manufacturing nanoparticles in a precise and controllable manner. However, the experimental optimization of microfluidic nanoparticle fabrication faces challenges related to the intricate interplay of various process parameters within the microscale environment. The integration of experiments and computational fluid dynamics (CFD) offers a synergistic approach that allows the researchers to validate and optimize theoretical models with real-world experimental models, enhancing the precision of nanoparticle synthesis and facilitating the design of more efficient microfluidic systems. This review provides a critical analysis of the current state of knowledge on recent advances of numerical investigations for nanoparticle synthesis using microfluidic-based methods. In particular, an overview of CFD assisted studies for microfluidic production of nanoparticles is presented, whilst their advantages and limitations are discussed. The importance of numerical modelling using CFD on the understanding of droplet generation, mixing and reaction mechanisms and how these phenomena are associated with nanoparticle nucleation and growth are highlighted. Different microfluidic-based approaches to produce uniform nanoparticles are presented and the most promising techniques are identified and discussed in detail. Both passive and active mixing microfluidic strategies are considered, highlighting their impact on nanoparticle formation. A comparative study of experimental and numerical approaches is performed to provide a better understanding of the droplet breakup mechanisms and the influence of physicochemical parameters on the size and shape of the produced nanoparticles. The review confirms that adoption of CFD simulations can be beneficial to identify critical flow conditions and reaction zones, which are essential for controlling the synthesis of nanoparticles. Finally, by systematically integrating CFD with experimentation, it will be possible to translate microfluidic nanoparticle synthesis into scalable and industrially viable technologies.

1. Introduction

Owing to their novel properties and potential applications, nanoparticles (NPs) have attracted increased attention in several fields, with the most popular being environmental, biomedicine, and electronics. Nanoparticle-based therapeutics become increasingly available to healthcare systems, since nanometre-sized particles are exceptional candidates as delivery vehicles in pharmaceutical industries, due to the subcellular particle size, good biocompatibility, and controlled release characteristics [1,2]. The global healthcare nanotechnology market was estimated at \$316 billion in 2023 and is growing at a CAGR (Compound Annual Growth Rate) of 15.1 % to reach \$556 billion by the end of 2027 with a total of 48 nanotechnology-related products being regulatory

approved and another 299 being in pre-clinical stage [3]. Amongst them, lipid nanoparticles (LNPs) loaded with mRNA molecules, have already been used in vaccines by Moderna and BioNTech/Pfizer to treat diseases, such as acute respiratory syndrome coronavirus 2 (SARS-CoV-2) and are already available in the market [4]. Nevertheless, the commercialization of nanoparticle- based therapeutics faces major challenges such as lack of quality control, efficient product purification, scalability, high manufacturing cost, product biocompatibility and toxicity, and therapeutic capacity.

The nanoparticles' structure and composition can significantly vary, depending on the materials used, which can be organic (such as lipids and polymers) or inorganic (such as silica and gold) [5]. Many studies have already extensively reviewed the types of nanoparticles used for

E-mail address: d.tsaoulidis@surrey.ac.uk (D. Tsaoulidis).

https://doi.org/10.1016/j.ceja.2025.100853

 $^{^{\}ast}$ Corresponding author.

drug delivery applications [6-8]; therefore, a detailed discussion of these is beyond the scope of the present work. The most commonly used synthesis methods include nanoprecipitation, high-shear homogenization, microemulsion, solvent injection and emulsification-solvent evaporation, which have been extensively described for different particle types [6-8]. The synthesis techniques typically involve two fundamental steps, i.e., nucleation and growth (Fig. 1A). Various theoretical frameworks have been developed to describe these processes [9-11], including the Classical nucleation and growth theory, the LaMer mechanism, the Ostwald ripening and Digestive Ripening, and the Finke-Watzky two-step mechanism. Table 1 provides an overview of the synthesis methods for polymeric, lipid-based, and inorganic nanoparticles, along with the theoretical models that describe their formation. Most of these methods are typically implemented in conventional batch systems, where nucleation and growth occur simultaneously [10]. The lack of control over the process stages, such as emulsion-solvent evaporation (Fig. 1B) during conventional bulk production processes, creates problems such as polydispersity, poor reproducibility, and a lack of precision in constructing sophisticated structures [12]. In contrast, the synthesis of nanoparticles in microfluidic devices via nanoprecipitation and emulsification enables decoupling of the nucleation and growth steps and accurate manipulation of process parameters. Microfluidics has emerged as a new approach to generate reproducible nanoparticle formulations and to address the challenges of current batch methods. Through increasing the surface area-to-volume ratio by several orders of magnitude, microfluidics provides rapid and uniform mass and heat transfer rates within the system [13,14]. Microfluidic devices are ideal candidates for the preparation of high-quality nanoparticles, providing high homogeneity, reproducibility, accurate control of reaction conditions, fast mixing, and low reagent consumption, as well as simplified fabricating processes [13].

Several review articles summarizing microfluidic methods for nanoparticle fabrication have been reported in the literature, providing an overview of existing microfluidic systems, and reaction mechanisms for the synthesis of various nanocarriers, such as lipid-based, polymer-based, protein-based, and inorganic formulations [10,15–29]. Highlighting the importance of microfluidic geometry, these articles describe how different microreactor configurations can improve the efficacy of drug delivery and generate nanoparticles of uniform size in a

Table 1
Summary of methods and mechanisms for polymer, lipid and inorganic nanoparticle synthesis.

Type of Nanoparticle type	Polymer	Lipid-based	Inorganic
Common synthesis methods	Nanoprecipitation, Emulsification/ Solvent evaporation, Solvent displacement	High-shear homogenization, Microemulsion, Solvent injection, Ultrasonication	Wet chemical synthesis (e.g., sol- gel, nanoprecipitation), thermal decomposition
Nucleation mechanism	LaMer	Crystallisation, self-assembly	Lamer mechanism, Classical Nucleation Theory (CNT)
Growth mechanism	Diffusion-limited growth	Coalescence	Ostwald ripening, diffusion
Theoretical models	Lamer, Population Balance Model (PBM), Classical Nucleation Theory (CNT)	Classical Nucleation Theory (CNT), Population Balance Model	Lifshitz-Slyozov- Wagner (LSW) model, Classical Nucleation Theory (CNT), Finke-
Applications	Targeted drug delivery, controlled drug release	(PBM), Delivery of mRNA and siRNA, Gene therapy	Watzky model Catalysis, Biosensors, Biomedical Imaging

reproducible manner. These review articles cover issues related with microfluidics, such as scale-up and fouling, and emphasize the need to accurately control and predict the flow patterns and physicochemical properties of the synthesized nanoparticles. Even though the use of microfluidics is at an advanced stage for nanoparticle synthesis, more insight needs to be provided on micro-scale production to obtain well-designed drug delivery systems. One of the most promising tools for future approaches is the utilization of numerical simulations, such as computational fluid dynamics (CFD) approaches, to optimize nanoparticle characteristics.

The current review focuses on the CFD methods applied to optimize fluidic conditions in microfluidic systems during nanofabrication. Recent advances in the field will be described in detail. The microfluidic techniques applied for nanoparticle synthesis will be described and the methods used to capture particle nucleation and growth will be

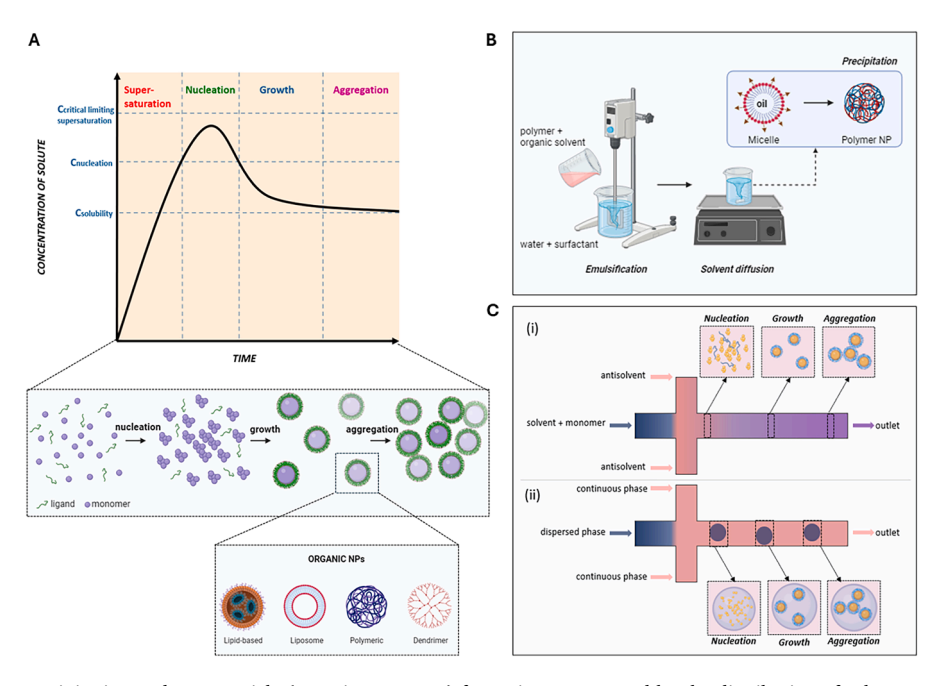


Fig. 1. (A) Progress of nanoprecipitation and nanoparticle (organic structures) formation represented by the distribution of solute concentration, (B) Batch-based production of polymer nanoparticles using emulsion diffusion method, (C) Nanoparticle formation in i) single-phase and ii) multiphase microfluidic systems.

provided. Subsequently, the importance of incorporating computational methods to analyse nanoparticle formation in microfluidic conditions will be highlighted. Overall, this article will provide insights into the flow dynamics within microfluidics systems, as predicted by CFD simulations, which enable precise control over nanoparticle synthesis.

Although polymeric, lipid-based, and inorganic nanoparticles are often grouped together as drug delivery carriers, their synthesis mechanisms and CFD modelling requirements differ significantly. Polymeric systems are typically prepared through nanoprecipitation or emulsification, where CFD is mainly used to analyse solvent-antisolvent mixing, diffusion-limited growth, and the effects of flow rate ratio on particle distribution [30]. Lipid-based formulations, rely on the self-assembly of amphiphilic molecules into bilayers or liposomes, with CFD to capture interfacial dynamics and amphiphile packing; coupling with population balance models (PBMs) is particularly useful for predicting vesicle size distributions [31]. Inorganic nanoparticles such as gold, silica, or iron oxide are generally produced through crystallisation or sol-gel reactions, where nucleation and growth are dominated by thermodynamic and kinetic factors (e.g., Ostwald ripening) [31]. For these systems, CFD resolves concentration and temperature gradients that drive supersaturation, while integration with kinetic models provides insight into crystallite size and morphology.

Taken together, this comparison underscores that while microfluidic flow control is central across all three classes, the dominant physicochemical processes, and thus the CFD strategies required, are material-specific. This suggests that future CFD studies should tailor model selection (e.g., continuum vs multiphase vs coupled CFD-PBM) to the nanoparticle type, rather than adopting a one-size-fits-all framework.

2. Microfluidic fabrication of nano-drug delivery systems

2.1. Nucleation and growth modelling

In nanomedicine-based therapy, NPs are used as carriers for delivering drugs, small interfering RNAs (siRNAs), and small molecular proteins. Their drug loading efficiency, controllable drug release, cellular toxicity, and stability are significantly affected by particle size, size distribution, shape, and composition [32]. Nanoparticle synthesis in microfluidics is achieved through precipitation from liquid solutions, which is described by the classical theory of nucleation and growth [11]. This process occurs when one solution, containing monomers, is mixed with an antisolvent and causes sudden changes in critical conditions, such as concentration or temperature, creating a supersaturated condition [10,11]. Classical nucleation theory (CTN) provided a foundational framework for the understanding of crystal nucleation and growth, where nucleation is considered to proceed through a single energy barrier [33]. The high Gibbs energy of a supersaturated solution triggers nucleation, where the monomers form a new structure of low energy (nuclei) which is thermodynamically favourable [10]. The total free energy (ΔG) in this system, is given by:

$$\Delta G = 4\pi r^2 \gamma + \frac{4}{3}\pi r^3 \Delta G_v \tag{1} \label{eq:deltaG}$$

where γ is the surface energy, r is the radius of a spherical particle and ΔG_v the crystal-free energy given by:

$$\Delta G_{v} = \frac{-k_{B}Tln(S)}{v} \tag{2}$$

where k_B is the Boltzmann's constant, S the degree of supersaturation in the solution and v its molar volume [9]. The rate of nucleation (dN/dt) can be expressed by the Arrhenius equation by:

$$\frac{\mathrm{dN}}{\mathrm{dt}} = \mathrm{Aexp} \left[-\frac{16\pi \gamma^3 \nu^2}{3 \mathrm{k_B}^3 \mathrm{T}^3 (\mathrm{lnS})^2} \right] \tag{3}$$

where A is the pre-exponential factor and T is the temperature. Based on

this equation it is indicated that nucleation depends on the temperature, the degree of supersaturation and the interfacial tension [34]. When the radius of a nucleus reaches to a critical value, $r_{C},\,\Delta G$ has a maximum value (energy barrier). At this point, the particles start to grow to reduce the free energy and reach a stable condition. Subsequently, growth of the NPs occurs, where monomers integrate into the surface of the nuclei, which may aggregate in case of insufficient stabilization of the formed NPs, resulting in further increase of the particle size [10,11]. Based on the classical growth theory, the growth of particles depends on the monomer's diffusion (Eq. (4)) to the surface or the surface reaction (Eq. (5)) and is modelled by:

$$\frac{dr}{dt} = \frac{Dv}{r} (C_b - C_r) \tag{4}$$

$$\frac{d\mathbf{r}}{dt} = k\mathbf{v}(\mathbf{C_b} - \mathbf{C_r}) \tag{5}$$

where r is the particle radius, k is the rate of surface reaction, C_b is the bulk concentration of monomers within the solution, D is the diffusion coefficient and C_r is the solubility of the particle [9].

2.2. Particle tracking and flow visualization in microfluidic systems

The development of microfluidic systems offers a new approach for precisely manipulating the manufacturing process and can be used to synthesize NPs in a highly controlled and reproducible way [3]. Controllable fabrication is enabled through real-time visualisation of the flow characteristics through various experimental techniques, such as 1) transmitted microscopy, 2) confocal microscopy (CLSM), 3) fluorescent microscopy, 4) microscopic particle image velocimetry (micro-PIV), and 5) Raman spectroscopy [35]. The most used method for focusing on a specific area in a micromodel at high resolution is incorporating high-speed cameras coupled with transmitted or reflected microscopes to capture images and videos of the flow (Fig. 2A). The CLSM and micro-PIV methods can be used for fluid and particle velocity measurements. The CLSM technique is used for high resolution requirements and observed displacements over a length scale less than the optical diffraction limit, while the PIV requires the fluid to be tagged with tracer particles that illuminate when subjected to a laser source (Fig. 2C). Similarly, in fluorescent microscopy, the fluid is dyed with fluorescent dye and a light source is utilized to excite the molecules, coupled with a digital camera to capture the light (Fig. 2B). However, this method is used for concentration measurements of the target analyte. For more detailed information on the kinetics, thermodynamics and mass transport of chemical structures, the Raman spectroscopy is applied, where the vibrational modes of molecules are measured (Fig. 2D). Even though these techniques have been widely applied for quantitative and qualitative analysis of the microfluidic systems, the insights provided are limited. This is due to advantaged attributed to each experimental technique, such as slow analysis speed, weak detection signals, overlapping of two imaged fields, excess fluorescence excitation, low sensitivity, short optical path length and lack of information for components that are out of plane in 2D measurements [36,37].

2.3. Nanoparticle production in single-phase systems

Microfluidics can be classified into single-phase and multiphase systems (Fig. 1C) [20]. In single-phase systems, nanoparticles are formed through precipitation. This is achieved through molecular interdiffusion in laminar flow streams, while chaotic advection can be generated to increase the interface between the fluids and improve mixing performance [42]. The mixing inside the microdevices can be improved either by using external energy (active design) or by creating secondary flows through complex geometrical patterns (passive design) [43]. Due to their ease of fabrication, passive microdevices have been widely used for nanofabrication. Commonly used passive designs

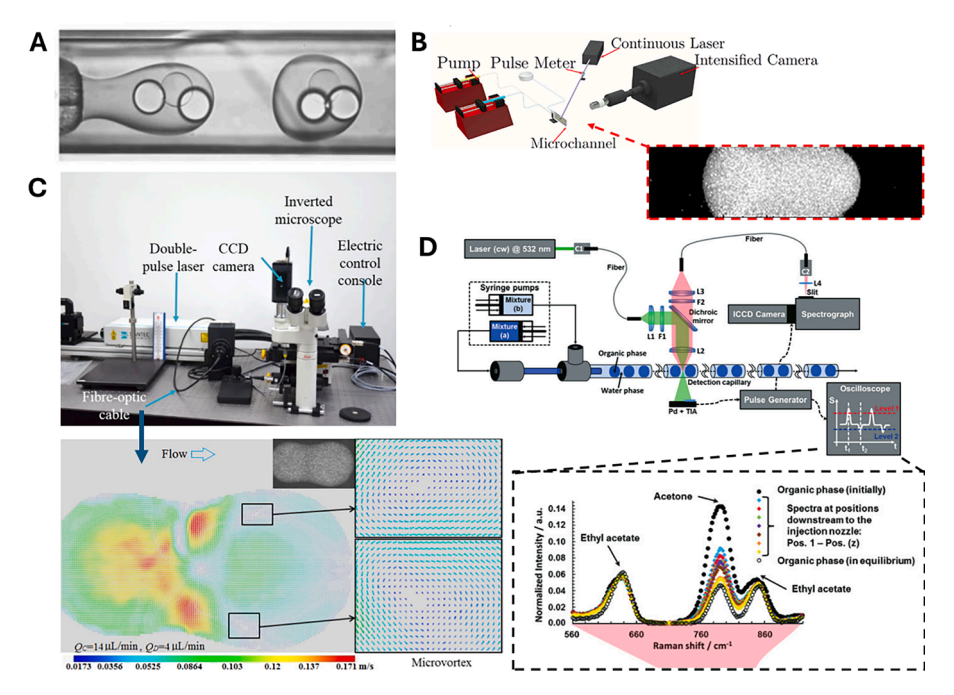


Fig. 2. Experimental methods for microfluidic flow visualization: (A)High-speed camera image of multiple droplet generation in microfluidic capillary tube [38], (B) Experimental setup for Laser Induced Fluorescence (LIF) measurements and images of the plug formed in a 200 µm quartz microchannel [39], (C) Experimental setup of Micro-PIV system and obtained velocity/microvortex profiles of two merging microdroplet [40], (D) Experimental setup of micro capillary device in-line with optical system and Raman spectra of the organic phase [41].

include T- or cross-shaped junctions (Fig. 3A and B), where the two phases are introduced through side channels to the main structure. Examples of more sophisticated designs include baffle mixers (Fig. 3C), which consist of repeated rectangular objects attached to the side walls of the channel, and staggered herringbone channels, which consist of V-shaped ridges (Fig. 3D). Currently, the majority of the research focuses on the development of microfluidic systems that allow rapid production of multifunctional nanoparticles with controllable properties. Therefore, attempts have been made to control the nanoparticle's nucleation and growth by adjusting the mixing time [44]. It has been shown that the mixing time is quadratically associated with the channel width and the flow rate ratio of the flows [42]. The smallest particle sizes

with good monodispersity are achieved when the mixing time is shorter than the nucleation time of nanoparticles [20]. Taking advantage of the small dimensions, microfluidics can greatly reduce the mixing time to milliseconds in the nucleation stage of NP synthesis [42].

Many continuous flow-based microfluidic systems have been employed to assess the quality of the nanoparticles, specifically their size, particle dispersity, and their ability to encapsulate bioactive compounds (i.e., encapsulation efficiency). The effects of the most dominant variables such as the total flow rate, flow rate ratio, composition of the solutions and reaction time on the desired properties have been thoroughly examined. Easily fabricated conventional structures of passive micromixers have been implemented, such as iLiNP devices (invasive

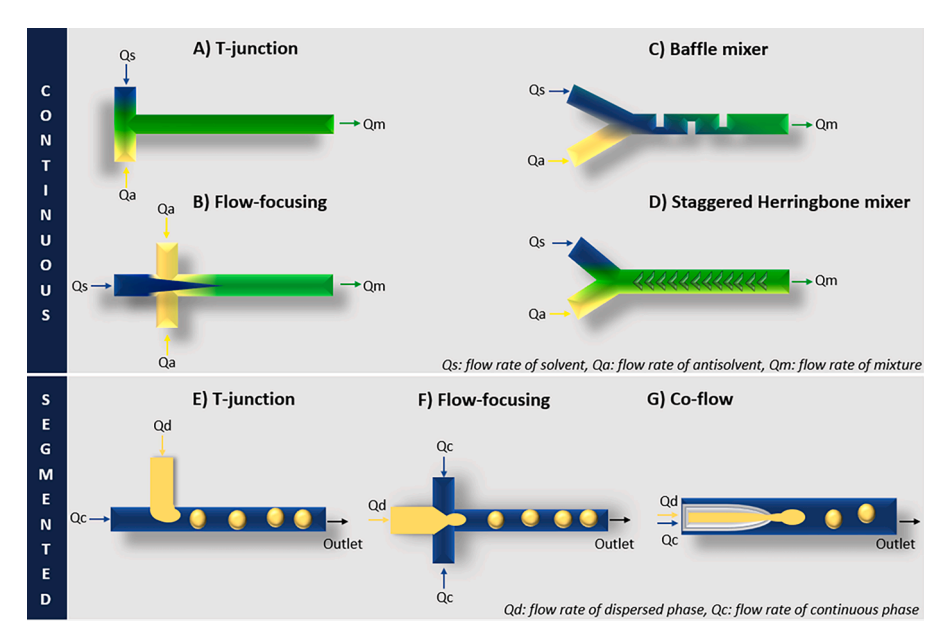


Fig. 3. Commonly used microfluidic structures for nanoparticle generation in continuous flow (single-phase systems) and segmented flow (multiphase systems).

lipid nanoparticle device) [45–47], which have a baffle mixer structure (Fig. 4A). Other passive designs include Y-shaped and curved or serpentine channels (Fig. 4B and C) [48-54], multi-vortex mixers (Fig. 4D), novel designs with multiple inlets [55-60], and capillary columns (Fig. 4F) [61,62]. In most cases, the nanoparticles generated are characterized by low polydispersity index (PDI) (PDI < 0.3) and size-tunable properties (< 200 nm), showing high dependence on the operating conditions, such as the channel geometry, residence time, and flow rates. However, it has not yet been fully understood how these operating conditions affect the resulting particle properties. Considering the high dose demand for nanoparticles in each therapeutic application and the inherent limitation of microfluidic devices to process large quantities, more studies should focus on developing scaling up strategies to increase the throughput of microfluidic systems, while maintaining accurate fluid handling and control. High throughputs (e.g., 320 mL/min) are achieved either by parallelizing devices (Fig. 4E) or by increasing the flow rate under chaotic advection conditions [55,57,59]. Recently, Giorello et al. [63], reviewed current microfluidic platforms utilized to develop scalable processes and suggested that a combination of both parallel devices and high total flow rates would be a promising strategy to increase productivity [63].

2.4. Nanoparticle production in multiphase systems

The synthesis of nanoparticles in multiphase systems occurs in discrete segments, created by two or more immiscible phases [69]. Depending on the interaction between the phases, droplets, slugs, or annular flows can be generated. Droplet-based microfluidics has been widely used for drug delivery applications, enabling the synthesis of highly monodispersed nanoparticles with controlled physicochemical properties. The droplets are isolated from each other and the channel walls, reducing the risk of channel clogging and improving the controllability of heat and mass transfer and reaction kinetics [70]. This technique not only enables biomolecule encapsulation into discrete droplets but also generates micro-carriers with high drug-loading capacity and sustained drug release, by modifying the internal structure of the droplets [71].

Droplet formation depends on the competition of interfacial tension and viscous shear stress at the interface of the two phases (Fig. 5A) [20, 72]. The shear stress, associated with the viscosity and the flow rate of two phases, determines the size of the droplets [73]. Depending on the wettability effects (Fig. 5B), the two phases can be discretised into the continuous phase, which is the fluid that completely or partially wets the microchannels, and the dispersed phase, which has no contact with the walls of the channel. Droplet generation and manipulation in microfluidic devices can be either active, requiring an external force, such as

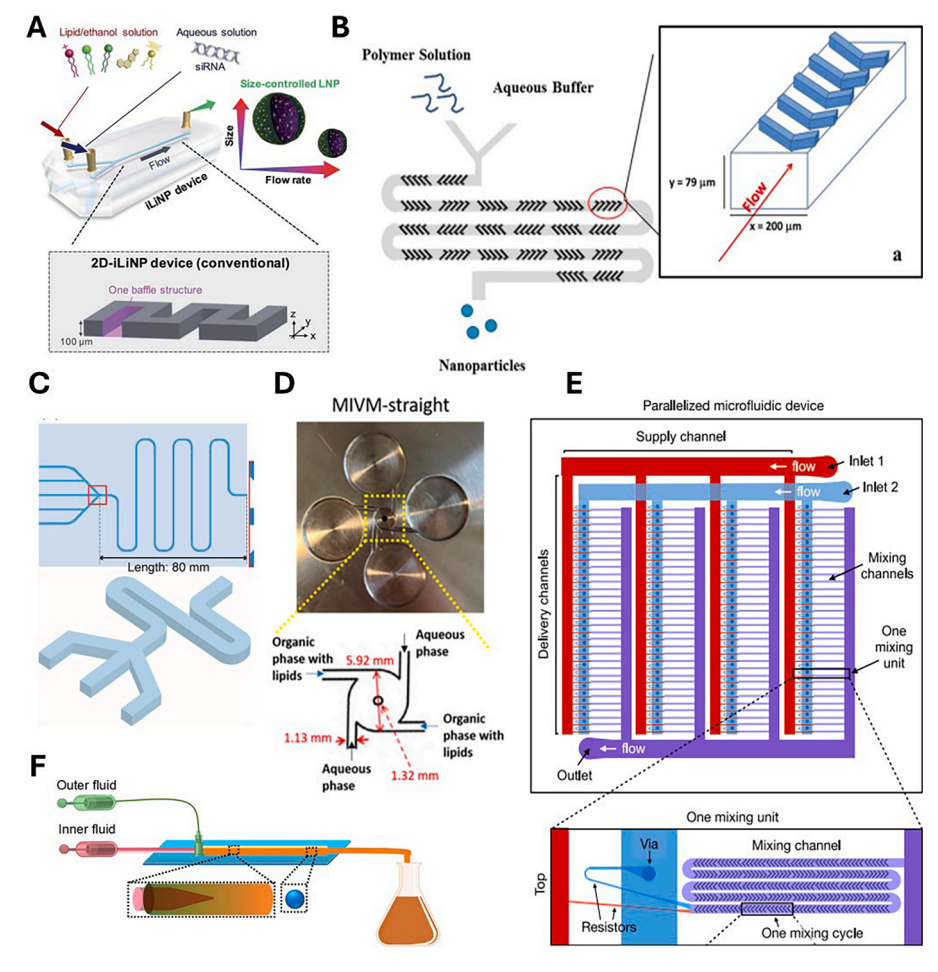


Fig. 4. (A) 3D view of iLiNP device with 20 baffle mixer designs to prepare 10 nm siRNA-loaded lipid nanoparticles. The device has 200 μm width and 100 μm height [64], (B) Staggered Herringbone micromixer (SHM) with a Y-shaped design and sequential regions of the herringbone structure to prepare poly(lactic-co-glycolic acid) copolymer (PLGA) nanoparticles [65], (C) PDMS iLiNP device with three inlets with straight structure and long channels [45], (D) Multi-inlet vortex mixer (MIVM) with 4 straight inlet channels fabricated with stainless steel. The two inlets of each phase are opposite, and the device is used for encapsulation in liposomes [66], (E) Parallelised microfluidic device with ladder design including 4 rows of 32 mixing units and flow resistors. The mixing unit has a staggered herringbone structure and is used to produce lipid nanoparticles [67] (F)3D-coaxial-flow microfluidic device consisting of two coaxial glass capillaries used to produce celecoxib NPs [68].

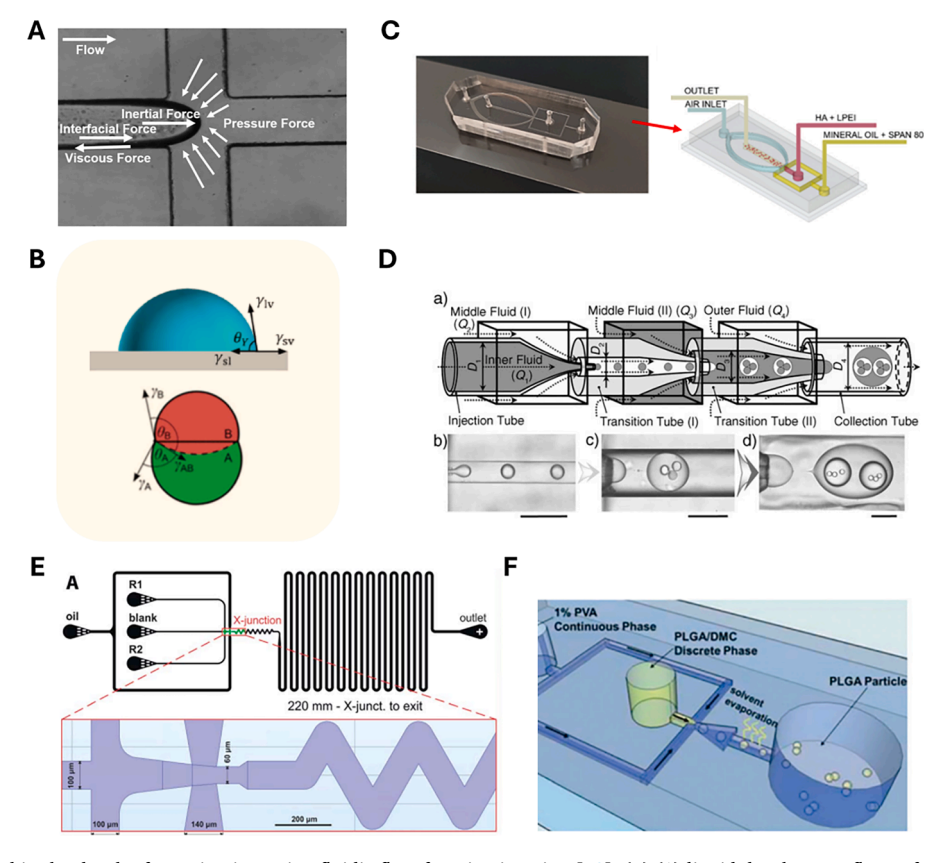


Fig. 5. (A) Forces involved in the droplet formation in a microfluidic flow-focusing junction [79], (B) (1) liquid droplet on a flat surface with the contact angle θ_{γ} , where γ_{lv} is the liquid-vapor interfacial tension, γ_{sl} is the solid-liquid interfacial tension and γ_{sv} is the solid-vapor interfacial tension [80](2) Double droplet consisting of phase A and B with their contact angles θ and interfacial tensions γ [81], (C)PDMS microfluidic device for droplet-based synthesis of polymer nanogels with flow focusing junctions [82], (D) a) Three microfluidic capillary tubes co-axially assembled for the preparation of triple emulsions b-d) High speed images of the emulsions produced in the first, second and third stage respectively [38], (E) PDMS microfluidic device for synthesis of iron oxide nanoparticles through droplet generation. It consists of four inlets. Droplets are produced in a flow focusing X-junction and are carried to the outlet through a meandering channel of 220 mm [83], (F) Microfluidic design for PLGA particle synthesis from droplets and solvent extraction method, including a flow focusing junction [84].

electric, magnetic, or acoustic force, or passive. In the case of passive designs, pressure-driven microdroplet generators are implemented, such as T- or Y-shaped (Fig. 3E) junctions and flow focusing junctions (cross-shaped) (Fig. 3F), integrated in serial and parallel manners, or capillary tube microreactors (Fig. 3G) constructed by assembling co-axially capillaries into tips with orifices of specific sizes [10,14]. A cross-shaped junction provides better control over the generated droplets than a T-shaped junction since the dispersed phase is symmetrically sandwiched by two streams of the continuous phase [74]. So far, the most efficient droplet-based devices for nanoparticle formation are chip-based flow focusing and capillary-based devices [12]. Microfluidic devices can be made of polymer, providing ease of fabrication, or glass which shows limited flexibility in the channel design [74]. However, glass devices provide better compatibility with organic solvents compared to most of the polymer microchips. Changing the material in each microfluidic system can alter the surface wettability, which provides nanoparticles with diverse properties according to their targeted therapeutic application.

Droplet-based microfluidics shows significant benefits compared to chaotic mixing by eliminating the need to control complicated flow patterns and minimizing dilution, and contamination problems [71]. Droplets can be used as microreactors for nanoparticle nucleation and growth and their properties (size, uniformity) can be controlled by optimizing the microfluidic design, the reagents, and the flow conditions [21]. Despite the numerous advantages, studies examining droplet generation for therapeutic applications are limited. In most of them, passive designs with multiple inlets (Fig. 5C) and capillary-based tubes (Fig. 4F) are used to increase productivity, allowing for redesign of the

tip dimensions in combination with other variables such as the flow rate ratio to control the droplet size [75–78]. Even though the droplet properties significantly affect the final particle properties, limited information is available regarding the mechanism underlying this process.

2.5. Active microfluidic mixing systems

While Sections 2.3 and 2.4 focused on passive microfluidic systems (single and multiphase), recent advances also highlight the role of active micromixing strategies, which use external forces to further enhance control over nanoparticle synthesis. Common actuation methods include acoustic, ultrasonic, electrokinetic, magnetic, and pneumatic forces. Although they are generally more effective than passive strategies, the need for additional components increases system complexity and cost, which can limit practicality and commercial translation [85]. A widely used approach is acoustic micromixing based on the inverse piezoelectric effect, where electrical signals generate mechanical vibrations. The mixing mechanism depends on the applied frequency: at low frequencies (<200 kHz), acoustic cavitation occurs, producing turbulence and vortices that enhance mixing, while at higher frequencies (>1 MHz), cavitation is absent and mixing is promoted by acoustic streaming and radiation forces, which disrupt laminar flow [31]. For example, Huang et al. (2019) used a PDMS microdevice combining acoustic actuation with sharp edges to produce PLGA and chitosan nanoparticles (Fig. 6A) [86]. By changing the frequency (~4 kHz) and edge length, they achieved particles of 88.6 nm with a PDI of 0.13. Similarly, Pourabed et al. (2022) designed a multilayer microfluidic device consisting of a silicon wafer sandwiched betweentwo PDMS layers and bonded to a

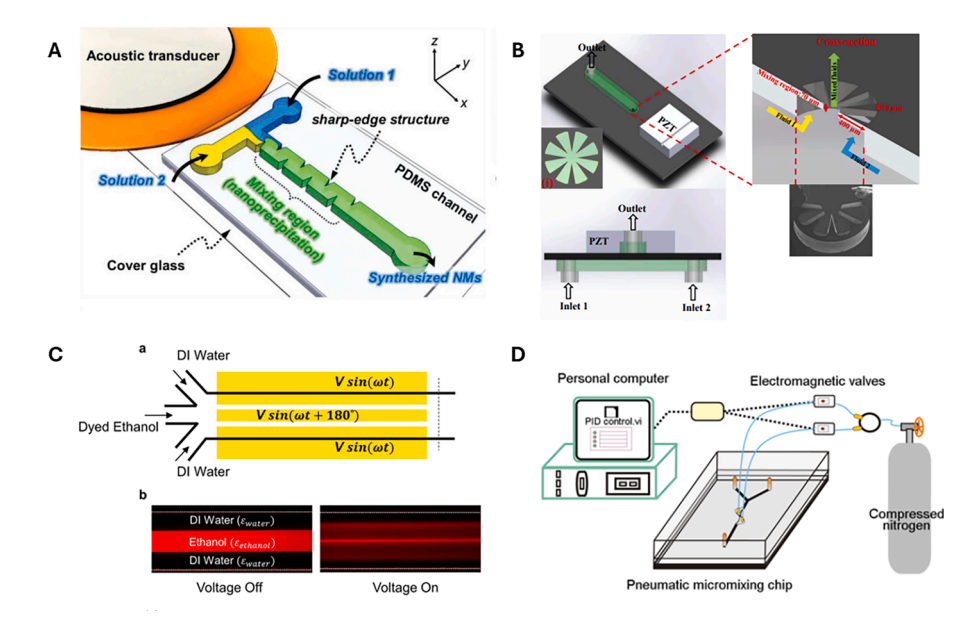


Fig. 6. (A) Schematic of the acoustofluidic synthesis device, consisting of a PDMS microchannel with multiple sharp-edge structures, a glass slide, and an acoustic transducer [86], (B)) Schematic of the microfluidic device with the piezoelectric disk and top view of Lotus shaped structure [87], (C) a) Schematic of the device geometry, electrode configuration, and voltage excitation. The outer electrodes were driven at the same amplitude (V) and frequency (ω), with the centre electrode at a 180° phase shift (b) Fluorescent images at the dashed line showing laminar streams of DI water and Rhodamine B dyed ethanol with voltage off and on [88], (D) Experimental setup of pneumatic micromixing system [89].

piezoelectric disk (Fig. 6B). In this design, fluids flow from the bottom channel through the silicon substrate into the top PDMS layer, where the silicon is etched into a circular "lotus" arrangement of sharp edges. Operating at high frequency (\sim 680 kHz), this system produced PLGA nanoparticles of 52 nm with a PDI of 0.44 [87].

Electrical micromixers represent another class of active devices, where embedded electrodes apply DC or AC fields to drive fluid motion. Mixing can occur via electrohydrodynamic (EHD) instabilities between fluids of different properties, or via AC electrothermal (ACET) effects in which local heating generates vortices. Using this approach, [88] synthesized cationic, anionic, and neutral liposomes in a PDMS-gold electrode system (Fig. 6C) [88]. Neutral DPPC-cholesterol liposomes averaged 126.7 ± 0.7 nm, while cationic and anionic liposomes were $91.8{\text -}109.1$ nm and of $100.4{\text -}114.6$ nm, respectively.

Active designs have also been applied for inorganic nanoparticle synthesis. Wang et al. [89] synthesized CdS quantum dots using a pneumatic microfluidic device with an "S"-shaped mixing chamber and vibrating diaphragm driven by compressed nitrogen (Fig. 6D) [89]. Incorporating sodium polyphosphate produced smaller and more uniform quantum dots than conventional co-precipitation under magnetic stirring.

Importantly, CFD is increasingly used to model the multiphysics interactions underpinning active micromixing, including acoustic streaming, electrohydrodynamic instabilities, and thermal gradients. Such models enable prediction of optimal actuation frequencies, electrode configurations, and device geometries, complementing experimental studies. Overall, active microfluidic mixers offer enhanced control of particle size and polydispersity compared to passive systems, though their performance depends strongly on the actuation method and device material.

3. Numerical modelling of microfluidic-assisted nanoparticle formation

A thorough understanding of the flow characteristics and transport phenomena during nanoparticle growth is necessary to better control the process in microfluidic systems. Considering the limitations of the current experimental methods used for flow visualisation,

Computational Fluid Dynamics (CFD) has evolved as a powerful numerical tool to offer insights into the flow characteristics in complex geometries. It has been widely used to describe and model hydrodynamic and thermal phenomena and consequently to optimize process design and operation [30,90]. CFD provides additional information on mixing mechanisms and droplet formation which would otherwise require advanced experimental studies, such as laser-based optical diagnostics. Accurate predictions on the concentration, velocity, and pressure profiles are used to identify the operating conditions that mostly impact the performance of the device and therefore facilitate optimal design of each microfluidic system [91-94]. An important consideration for translation to industrial practice is the interplay between CFD simulations and experimental validation, particularly for process scale-up. While experimental studies remain indispensable for validation, CFD allows systematic evaluation of operating conditions and device geometries that are difficult to perform experimentally [95, 96]. When combined, these approaches enhance process controllability, accelerate optimization, and reduce development costs, thereby facilitating the translation of microfluidic systems to higher throughputs. This integrated strategy creates a predictive framework for scale-up, enabling computational pre-screening of designs and operating windows before experimental implementation.

The most common numerical methods used in CFD studies are the finite element method (FEM) and finite volume method (FVM) [97]. In the case of immiscible two-phase systems, models such as the volume of fluid method (VOF), the level-set method (LSM), the Lattice-Boltzmann method (LBM) and the phase field method are adopted [97]. The VOF and LSM methods solve the Navier-Stokes equations for macroscopic variables, such as velocity, pressure, and density to capture the interface between different fluids [98]. These two models are based on the sharp-interface assumption, where the interface between the different fluids is considered of zero thickness [99]. While the VOF method, is described by transport equations of the mass fraction function in a specified volume, the LS method applies free-surface boundary conditions and uses the function φ [100]. This function expresses the distance from the interface and takes negative values in one phase and positive values in the second phase, with 0 being the value at the interface [101]. Even though the LS method makes it easier to incorporate surface

tension, it is not mass-conservative. For that reason, it has recently become common to combine both VOF and LS methods (Coupled Level Set and Volume of Fluid). On the other hand, the LBM describes the dynamics of particle distribution confined to a regular space-time lattice according to Boltzmann kinetic equations [97]. Unlike the VOF and LS methods, in the LBM analysis, the interface is not tracked explicitly but results from the thermodynamic foundation of the method [102]. The phase field model is based on the idea that the interface between two fluids is a layer of finite thickness rather than a sharp discontinuity. In both LBM and phase-field methods, a high numerical resolution is necessary to model real interface thickness [99].

The majority of the CFD work on microfluidics is dated after 2010, where several research groups have applied CFD simulations in their studies to examine flow patterns that are affected by fluid properties (e. g., viscosity, surface tension, and density), channel geometry, and operating conditions (flow rates and flow rate ratio) during nanoparticle formation in microfluidic systems for drug delivery applications. Some groups focused the numerical analysis on the investigation of the optimal geometric design for improved mixing efficiency [83,103,104], whilst others studied the characterization of the mixing intensity and droplet generation mechanism during nanoparticle formation [66–72]. The CFD results were generally in good agreement with experimental work (<10 % deviation) and enabled the development of models used for the selection of optimal operating parameters of the microfluidic platforms [104]. A summary of the CFD-assisted studies focusing on microfluidic nanofabrication is presented in Table 2.

Coupled with computational fluid dynamics (CFD), the Population Balance Model (PBM) has become a powerful tool for simulating lipid and polymer nanoparticle formation in microfluidic systems. PBMs are formulated using balance equations that track the evolution of the particle size distribution (PSD) accounting for key phenomena such as nucleation, growth and aggregation [105]. Common numerical methods for solving PBMs within CFD frameworks include the class method (CM), quadrature method of moments (QMOM), and the direct quadrature method of moments (DQMOM) [106]. The CM discretizes the particle size domain into a finite number of size classes and solves the governing equations for each class, providing a detailed PSD but at a high computational cost. QMOM approximates the PSD using a finite set of moments and the associated quadrature weights, offering computational efficiency but without direct access to the full distribution. DQMOM, an extension of QMOM, enables more accurate tracking of PSD evolution, especially in the presence of complex phenomena like aggregation. By combining CFD with PBM solvers, it becomes possible to analyse critical fields within the mixing zone, such as mass fraction gradients, mixing time, local supersaturation, and mean particle size, which are essential for understanding and predicting nanoparticle precipitation dynamics. Several numerical studies have successfully employed these coupled methods to provide insights on how operating conditions affect supersaturation profiles and ultimately control nucleation and growth in microfluidic systems [105,107–112].

While the numerical methods discussed above have been extensively applied to drug delivery, CFD modelling of nanoparticle behaviour is equally relevant in other fields where microdevice optimization and precise control are required. For example, in environmental engineering, CFD has been used to study nanoparticle aggregation, dispersion, and transport in nanofluids, where enhanced thermal conductivity improves heat transfer and reduces energy consumption [113,114]. In groundwater remediation, nanoparticles such as zerovalent iron or metal oxides have been employed for contaminant adsorption, and CFD simulations have provided valuable insights into their dispersion in porous media and interactions with pollutants [115]. These examples show that the same modelling approaches that guide drug delivery can be generalized to environmental nanotechnology, underscoring the broad applicability of CFD in tailoring nanoparticle performance across diverse domains.

 Table 2

 CFD-assisted literature for microfluidic production of nanoparticles.

design Effect of micromixing mechanism in the particle size Effect of process parameters (velocity profile, biomass concentration, temperature) in size distribution Effect of the complex interplay between molecular and fluid dynamic properties of precipitating species Analysis of mixing process in the vicinity of microfluidic orifice Validation of experiments Characterization of fluid pattern in microfluidic device Analysis of the hydrodynamic process and its implication for the polymeric NPs formation Effect of the fluid flow properties isosurface of zein NP coacervation. Analysis of the concentration and velocity fields in the microfluidic domain Effect of flow rate on nanoparticle size Influence of channel height on mixing performance within the droplets Selection of optimal mixing efficiency conditions Analysis of droplet generation mechanism Selection of optimal microfluidic device for controllable manoparticle synthesis Prediction of optimal geometry design for fouling prevention Effect of process in the vicinity of microfluidic device (mixing-based) Nove 3D micromixer 2012 [117 design T-junction (mixing based) Flow focusing Y-junction (mixing-based) Co-flow capillary device (mixing-based) Co-flow capillary device 2015 [30] (mixing-based) Co-flow capillary device 2015 [44] (mixing-based) Y-, T- & cross junction 2016 [96] (droplet-based O/W) Mixing in sequential 2017 [90] (apilor device of channel height on mixing performance within the droplets in flow focusing (mixing-based) Mixing-based) Mixing-based) Mixing inside droplets in 2021 [123 and policy device (mixing-based) Mixing inside droplets in 2021 [124 and policy device (mixing-based) Mixing inside droplets in 2021 [125 and policy device (mixing-based) Mixing-based) Mixing-based) Mixing-based) Mixing inside droplets in 2021 [126 and policy device (mixing-based) Mixing-based) Mixing-based) Mixing inside droplets in 2021 [126 and policy device (mixing-based) Mixing-based) Mixing-based) Mixing-based) Mixing-based	CFD-assisted literature for microfluidic production of nanoparticles.								
Selection of optimal micromixer design Effect of micromixing mechanism in the particle size Effect of process parameters (velocity profile, biomass concentration, temperature) in size distribution Effect of the complex interplay between molecular and fluid dynamic properties of precipitating species Analysis of mixing process in the vicinity of microfluidic orifice (mixing-based) Characterization of fluid pattern in microfluidic device (mixing-based) Characterization of fluid pattern in microfluidic device (mixing-based) Analysis of the hydrodynamic process and its implication for the polymeric NPs formation Effect of the fluid flow properties isosurface of zein NP coacervation. Effect of geometry on the characteristics of pressure drop and flow field Calculation of mixing time Effect of flow rate on nanoparticle size Influence of channel height on mixing performance within the droplets Selection of optimal mixing efficiency conditions Analysis of droplet generation mechanism Selection of optimal microfluidic device for controllable manoparticle synthesis Prediction of potimal geometry design for fouling prevention Effect of process parameters on droplet generation and droplet characteristics	CFD analysis		•	Year	Ref				
Selection of optimal micromixer design Effect of micromixing mechanism in the particle size Effect of process parameters (velocity profile, biomass concentration, temperature) in size distribution Effect of the complex interplay between molecular and fluid dynamic properties of precipitating species Analysis of mixing process in the vicinity of microfluidic device Analysis of the hydrodynamic process and its implication for the polymeric NPs formation Effect of geometry on the characteristics of pressure drop and flow field Calculation of mixing time Effect of flow rate on nanoparticle size and PDI Selection of optimal mixing of rof fouling prevention Effect of process parameters on droplet generation and droplet characteristics T-junction (mixing based) Co-flow capillary device (mixing-based) V-, T- & cross junction 2016 [96] (droplet-based O/W) Mixing in sequential 2017 [90] Effect of geometry on the characteristics of pressure drop and flow field Calculation of mixing time Solection of optimal mixing efficiency conditions Analysis of droplet generation mechanism Selection of optimal mixing efficiency conditions Analysis of droplet generation for fouling prevention Effect of geometry design for fouling prevention				2011	[93]				
Effect of process parameters (velocity profile, biomass concentration, temperature) in size distribution Effect of the complex interplay between molecular and fluid dynamic properties of precipitating species Analysis of mixing process in the volumer of zein NP coacervation. Analysis of the concentration and velocity fields in the microfluidic domain Effect of geometry on the characteristics of pressure drop and flow field Calculation of mixing time Effect of flow rate on nanoparticle size Influence of channel height on mixing performance within the droplets Selection of optimal mixing efficiency conditions Analysis of droplet generation mechanism Selection of optimal microfluidic device for controllable nanoparticle synthesis Prediction of process parameters on droplet generation and droplet characteristics Velocity fields in an anoparticle size and PDI Selection of optimal geometry design for fouling prevention Effect of process parameters on droplet generation and droplet characteristics Vo-flow capillary device (mixing-based) Co-flow capillary device (mixing-based) V-, T- & cross junction (droplet, based) V-, T- & cross junction (droplet aparticle synthesis T-junction & Flow (coll device design (droplet-based) Mixing in sequential capillary devices V-shaped micromixer 2018 Effect of flow rate on nanoparticle size Droplet based Internal mixing of droplet spensation Mixing-based) Mixing inside droplets in 3D capillary device V-junction including based) Mixing inside droplets in 3D capillary device V-junction including based) Mixing inside droplets in 3D capillary device V-junction including based) Mixing inside droplets in 3D capillary device V-junction including Dased) Dased in the microfluidic droplet generation Mixing-based) Mixing inside droplets in 3D capillary device V-junction including Dased Dased in the microfluidic Mixing-based Mixing inside droplets in Dased in the microfluidic Mixing-based Mixing inside droplets in Mixing inside droplets in Dased in the microfluidic Mixing-based Mix	Selection of optimal micromixer		T-junctions (mixing	2011	[104]				
Effect of process parameters (velocity profile, biomass concentration, temperature) in size distribution Effect of the complex interplay between molecular and fluid dynamic properties of precipitating species Analysis of mixing process in the vicinity of microfluidic orifice Validation of experiments Characterization of fluid pattern in microfluidic device Analysis of the hydrodynamic process and its implication for the polymeric NPs formation Effect of the fluid flow properties isosurface of zein NP coacervation. Analysis of the concentration and velocity fields in the microfluidic domain Effect of geometry on the characteristics of pressure drop and flow field Calculation of mixing time Effect of flow rate on nanoparticle size in mixing performance within the droplets Selection of optimal mixing efficiency conditions Analysis of droplet generation mechanism Selection of optimal microfluidic device for controllable nanoparticle synthesis Prediction of optimal geometry design for fouling prevention Effect of process parameters on droplet generation and droplet characteristics T-junction (mixing -based) Co-flow capillary device (mixing-based) Co-flow capillary device (mixing-based) Mixing in sequential 2017 [90] (mixing-based) Mixing in sequential 2017 [90] Effect of geometry on the characteristics of pressure drop and flow field Calculation of mixing time 3D co-axial flow focusing (mixing-based) Flow focusing junction- 2019 [122 proplet based in the mixing of droplets in flow focusing Mixing inside droplets in flow focusing with a wire 2021 [123 proplet based in the droplets in flow focusing 4 proplets 4 prop	Effect of micromixing mechanism in			2012	[116]				
Effect of the complex interplay between molecular and fluid dynamic properties of precipitating species Analysis of mixing process in the vicinity of microfluidic orifice Validation of experiments Co-flow capillary device (mixing-based) Characterization of fluid pattern in microfluidic device Analysis of the hydrodynamic process and its implication for the polymeric NPs formation Effect of the fluid flow properties isosurface of zein NP coacervation. Effect of geometry on the characteristics of pressure drop and flow field Calculation of mixing time Iffect of flow rate on nanoparticle size Influence of channel height on mixing performance within the droplets Selection of optimal mixing efficiency conditions Analysis of droplet generation mechanism Prediction of potimal geometry design for foulling prevention Effect of process parameters on droplet generation and droplet characteristics Flow focusing Y-junction (mixing ty-junction (mixing-based) Co-flow capillary device (mixing-based) Co-flow capillary device (mixing-based) Co-flow capillary device (mixing-based) Co-flow capillary device (mixing-based) V-, T- & cross junction 2016 [96] (droplet-based O/W) Italiant device for consumation and flow flow flow flow flow flow flow flow	Effect of process parameters (velocity profile, biomass concentration, temperatur		T-junction (mixing	2012	[117]				
Analysis of mixing process in the vicinity of microfluidic orifice Validation of experiments Co-flow capillary device (mixing-based) V-, T- & cross junction 2016 [96] Forcess and its implication for the polymeric NPs formation Effect of the fluid flow properties isosurface of zein NP coacervation. Effect of the fluid flow properties isosurface of zein NP coacervation. Analysis of the concentration and velocity fields in the microfluidic domain Effect of geometry on the characteristics of pressure drop and flow field Calculation of mixing time Effect of flow rate on nanoparticle size Influence of channel height on mixing performance within the droplets Selection of optimal mixing efficiency conditions Analysis of droplet generation mechanism Selection of optimal microfluidic device for controllable nanoparticle synthesis Prediction of nanoparticle size and PDI Selection of optimal geometry design for fouling prevention Effect of process parameters on droplet generation and droplet characteristics	Effect of the complex interp between molecular and fl dynamic properties of			2012	[118]				
Validation of experiments Co-flow capillary device (mixing-based) Characterization of fluid pattern in microfluidic device Analysis of the hydrodynamic process and its implication for the polymeric NPs formation Effect of the fluid flow properties isourface of zein NP coacervation. Analysis of the concentration and velocity fields in the microfluidic domain Effect of geometry on the characteristics of pressure drop and flow field Calculation of mixing time Effect of flow rate on nanoparticle size Influence of channel height on mixing performance within the droplets Selection of optimal mixing efficiency conditions Analysis of droplet generation mechanism Selection of optimal microfluidic device for controllable nanoparticle synthesis Prediction of optimal geometry design for fouling prevention Effect of process parameters on droplet generation and droplet characteristics Co-flow capillary device (mixing-based) (mixing-based) T-, T. & cross junction 2016 [96] (droplet-based O/W) Analysis of the hydrodynamic y. T. Flow focusing in sequential capillary device y. T. Flow focusing junction 2019 [122] Daffect of flow rate on nanoparticle size in flow focusing w. J. Junction 2019 [122] Selection of optimal mixing of droplets in flow focusing device y. Junction including 2021 [123] Belection of optimal geometry design for fouling prevention (mixing-based) Flow focusing device (mixing-based) Micromixer with a wire 2021 [126] Selection of optimal geometry design for fouling prevention (mixing-based) Effect of process parameters on droplet generation and droplet generation generation generation generation generation generation generation	Analysis of mixing process i			2014	[119]				
Characterization of fluid pattern in microfluidic device (mixing-based) Analysis of the hydrodynamic process and its implication for the polymeric NPs formation Effect of the fluid flow properties isosurface of zein NP coacervation. Analysis of the concentration and velocity fields in the microfluidic domain Effect of geometry on the characteristics of pressure drop and flow field Calculation of mixing time Effect of flow rate on nanoparticle size Influence of channel height on mixing performance within the droplets Selection of optimal mixing efficiency conditions Analysis of droplet generation mechanism Selection of optimal microfluidic device for controllable nanoparticle synthesis Prediction of optimal geometry design for fouling prevention Effect of process parameters on droplet generation and roplet generation and roplet characteristics Co-flow capillary device (mixing-based) Y-, T- & cross junction (droplet-based O/W) T-junction & Flow (droplet-based) Mixing in sequential 2017 [90] Mixing in sequential 2017 [90] T-shaped micromixers 2018 [121] 2018 [121] 2019 [68] (mixing-based) Effect of flow rate on nanoparticle (mixing-based) Internal mixing of 2020 [83] T-shaped micromixer 2021 [123] Mixing inside droplets in 2021 [124] Solution of optimal microfluidic 42 (mixing-based) Prodiction of nanoparticle size and PDI Selection of optimal geometry design for fouling prevention (mixing-based) Effect of process parameters on 4 (mixing-based) Effect of process parameters on 4 (mixing-based) 2D-Flow focusing device 2022 [127]	•		Co-flow capillary device	2015	[30]				
Analysis of the hydrodynamic process and its implication for the polymeric NPs formation Effect of the fluid flow properties isosurface of zein NP coacervation. Analysis of the concentration and velocity fields in the microfluidic domain Effect of geometry on the characteristics of pressure drop and flow field Calculation of mixing time Effect of flow rate on nanoparticle size Influence of channel height on mixing performance within the droplets Selection of optimal mixing efficiency conditions Analysis of droplet generation mechanism Selection of optimal microfluidic device for controllable nanoparticle synthesis Prediction of optimal geometry design for fouling prevention Effect of flow case and its implication for the polymeric NPs formation (droplets sheed (droplet based O/W) T-junction & Flow (droplet based (droplet based) T-junction & Flow (and proplet based) Teleptor of cousing junction-proplet based Internal mixing of droplets in flow focusing device (mixing-based) Effection of optimal microfluidic device for controllable paffle structure (mixing-based) Prediction of nanoparticle size and PDI Selection of optimal geometry design for fouling prevention Effect of process parameters on droplet generation and droplet characteristics		tern in	Co-flow capillary device	2015	[44]				
Effect of the fluid flow properties isosurface of zein NP coacervation. Analysis of the concentration and velocity fields in the microfluidic domain Effect of geometry on the characteristics of pressure drop and flow field Calculation of mixing time Effect of flow rate on nanoparticle size Influence of channel height on mixing performance within the droplets Selection of optimal mixing efficiency conditions Analysis of droplet generation mechanism Selection of optimal microfluidic device for controllable nanoparticle synthesis Prediction of optimal geometry design for fouling prevention Effect of speece of characteristics T-junction & Flow focused design (droplets based) Mixing in sequential 2017 [90] Tyshaped micromixers T-junction & Flow focused design (droplets based) in the properties and policy applies and policy in the properties and policy and policy applies and policy and policy applies applies and policy applies and policy applies applies and policy applies app	process and its implication		Y-, T- & cross junction	2016	[96]				
Analysis of the concentration and velocity fields in the microfluidic domain Effect of geometry on the characteristics of pressure drop and flow field Calculation of mixing time Effect of flow rate on nanoparticle size Influence of channel height on mixing performance within the droplets Selection of optimal mixing efficiency conditions Analysis of droplet generation mechanism Selection of optimal microfluidic device for controllable nanoparticle synthesis Prediction of optimal geometry design for fouling prevention Effect of process parameters on droplet generation and droplet generation and droplet generation and droplet generation droplet generation and droplet generation droplet generation and droplet generation droplet generation of optimal geometry design for fouling prevention Effect of geometry on the capillary devices Y-shaped micromixer 2019 [122] Solocaxial flow focusing generation application focusing device (mixing-based) Effect of flow rate on nanoparticle flow focusing device applications (mixing-based) Effect of process parameters on droplet generation and droplet characteristics	Effect of the fluid flow prop		focused design (droplet-	2017	[120]				
Effect of geometry on the characteristics of pressure drop and flow field Calculation of mixing time Effect of flow rate on nanoparticle size Influence of channel height on mixing performance within the droplets Selection of optimal mixing efficiency conditions Analysis of droplet generation mechanism Selection of optimal microfluidic device for controllable nanoparticle synthesis Prediction of optimal geometry design for fouling prevention Effect of geometry on the characteristics Y-shaped micromixer 2019 [122] Mixing inside droplets in 2021 [123] Mixing inside droplets in 2021 [124] Micromixer with a wire 2021 [125] Micromixer with a wire 2021 [126] Selection of optimal geometry design for fouling prevention (mixing-based) Effect of process parameters on droplet generation and droplet characteristics	velocity fields in the micr		Mixing in sequential	2017	[90]				
Calculation of mixing time Effect of flow rate on nanoparticle size Influence of channel height on mixing performance within the droplets Selection of optimal mixing efficiency conditions Analysis of droplet generation mechanism Selection of optimal microfluidic device for controllable nanoparticle synthesis Prediction of optimal geometry design for fouling prevention Effect of flow rate on nanoparticle size and droplet generation and droplet generation and droplet generation PDI Selection of optimal geometry design for fouling prevention Effect of process parameters on droplet generation and droplet characteristics Jocapilary device Y-junction including baffle structure (mixing-based) Micromixer with a wire coil 2021 [126] Micromixer with a wire coil 2022 [103] Effect of process parameters on droplet generation and droplet characteristics	Effect of geometry on the characteristics of pressure	drop	Y-shaped micromixers	2018	[121]				
Effect of flow rate on nanoparticle size Influence of channel height on mixing performance within the droplets in flow focusing Maring performance within the droplets in flow focusing Maring efficiency conditions Analysis of droplet generation mechanism Selection of optimal microfluidic device for controllable nanoparticle synthesis Prediction of optimal geometry design for fouling prevention Effect of process parameters on droplet generation and droplet generation and droplet generation of optimal geometry design for fouling prevention Effect of process parameters on droplet generation and droplet characteristics			_	2019	[68]				
Influence of channel height on mixing performance within the droplets in flow focusing X-junction Selection of optimal mixing (mixing-based) Analysis of droplet generation mechanism Selection of optimal microfluidic device for controllable nanoparticle synthesis Prediction of nanoparticle size and PDI Selection of optimal geometry design for fouling prevention Effect of process parameters on droplet generation and droplet characteristics Internal mixing of droplets in 2021 [123] Micromixer mixing-based) Prediction of nanoparticle size and micromixer with a wire 2021 [126] Selection of optimal geometry design for fouling prevention (mixing-based) Effect of process parameters on droplet generation and droplet characteristics	-	article	Flow focusing junction-	2019	[122]				
Selection of optimal mixing efficiency conditions Analysis of droplet generation mechanism Selection of optimal microfluidic device for controllable nanoparticle synthesis Prediction of nanoparticle size and PDI Selection of optimal geometry design for fouling prevention Effect of process parameters on droplet generation and droplet characteristics T-shaped micromixer (mixing-based) 2021 [123 2021 [124 2021 [125 2021 [126 2021 [126 2022 [103 2021 [126 2022 [103 2021 [126 2022 [103 2021 [126 2022 [103 2022 [103 2022 [127 2022 [127 2022 [127 2022 [127 2022 [127 2022 [127 2022 [127 2022 [127 2022 [127 2022 [127 2022 [127 2022 [127 2022 [127 2022 [127 2022 [127 2022 [127 2022 [127 2022 [127 2022 [127 2022 [127 2022 [127 2022 [127 2022 [127 2022 [127 2022 [127 2022 [127 2022 [127 2022 [127 2022 [127 2022 [127 2022 [127 2022 [127 2022 [127 2022 [127 2022 [127 2022 [127 2022 [127 2022 [127 2022 [127 2022 [127 2022 [127 2022 [127 2022 [127 2022 [127 2022 [127 2022 [127 2022 [127 2022 [127 2022 [127 2022 [127 2022 [127 2022 [127 2022 [127 2022 [127 2022 [127 2022 [127 2022 [127 2022 [127 2022 [127 2022 [127 2022 [127 2022 [127 2022 [127 2022 [127 2022 [127 2022 [127 2022 [127 2022 [127 2022 [127 2022 [127 2022 [127 2022 [127 2022 [127 2022 [127 2022 [127 2022 [127 2022 [127 2022 [127 2022 [127 2022 [127 2022 [127 2022 [127 2022 [127 2022 [127 2022 [127 2022 [127 2022 [127 2022 [127 2022 [127 2022 [127 2022 [127 2022 [127 2022 [127 2022 [127 2022 [127 2022 [127 2022 [127 2022 [127 2022 [127 2022 [127 2022 [127 2022 [127 2022 [127 2022 [127 2022 [127 2022 [127 2022 [127 2022 [127 2022 [127 2022 [127 2022 [127 2022 [127 2022 [127 2022 [127 2022 [127 2022 [127 2022 [127 2022 [127 2022 [127 2022 [127 2022 [127 2022 [127 2022 [127 2022 [127 2022 [127 2022 [127 2022 [127 2022 [127 2022 [127 2022 [127 2022 [127 2022 [127 2022 [127 2022 [127 2022 [127 2022 [127 2022 [127 2022 [127 2022 [127 2022 [127 2022 [127 2022 [127 2022 [127 2022 [127 2022 [127 2022 [127 2022 [127 2022 [127 2022 [127 2022 [127 2022 [127 2022 [127 2022 [127	Influence of channel height mixing performance with		Internal mixing of droplets in flow focusing	2020	[83]				
Analysis of droplet generation mechanism 3D capillary device Selection of optimal microfluidic device for controllable nanoparticle synthesis based) Prediction of nanoparticle size and PDI coil Selection of optimal geometry design for fouling prevention (mixing-based) Effect of process parameters on droplet generation and droplet characteristics Mixing inside droplets in 2021 [126 Wiczonizer with a wire coil 3D flow focusing device 2022 [103 Ginzing inside droplets in 2021 [126 Wixing inside droplets in 2021 [126 Wixing inside droplets in 2021 [126 Wixing inside droplets in 2021 [125 Dafflet structure (mixing-based) Wicromixer with a wire coil (mixing-based) 2D-Flow focusing device 2022 [127 droplet generation and droplet generation	Selection of optimal mixing		T-shaped micromixer	2021	[123]				
device for controllable nanoparticle synthesis based) Prediction of nanoparticle size and PDI coil Selection of optimal geometry design for fouling prevention (mixing-based) Effect of process parameters on droplet generation and droplet characteristics baffle structure (mixing-based) Micromixer with a wire 2021 [126 coil Micromixer with a wire 2021 [126 coil Coil 2022 [103 (mixing-based) 2D-Flow focusing device 2022 [127 droplet generation]	Analysis of droplet generation		Mixing inside droplets in	2021	[124]				
Prediction of nanoparticle size and PDI coil Selection of optimal geometry design for fouling prevention (mixing-based) Effect of process parameters on droplet generation and droplet characteristics Micromixer with a wire 2021 [126 coil 3D flow focusing device 2022 [103 (mixing-based) 2D-Flow focusing device 2022 [127 droplet generation	device for controllable	uidic	baffle structure (mixing-	2021	[125]				
for fouling prevention (mixing-based) Effect of process parameters on droplet generation and droplet characteristics (mixing-based) 2D-Flow focusing device- 2022 [127] droplet generation	Prediction of nanoparticle s	ze and	Micromixer with a wire	2021	[126]				
Effect of process parameters on droplet generation and droplet characteristics 2D-Flow focusing device- 2022 [127] droplet generation		y design	· ·	2022	[103]				
	Effect of process parameters droplet generation and dr		2D-Flow focusing device-	2022	[127]				
		aviour	Multi-inlet vortex mixer	2022	[66]				
Effect of physicochemical Vortex mixer 2022 [128 parameters on nanoparticle size and homogeneity	parameters on nanopartic	le size	Vortex mixer	2022	[128]				
Selection of optimal microdevice 2D &3D passive 2022 [94] micromixers		evice		2022	[94]				
		nation	Capillary device (droplet-	2022	[129]				
		ion	Flow focusing device	2022	[130]				
		on	T-junction (mixing-	2023	[131]				
	Analysis of device performa		3D nozzle-focused microchannel (droplet-	2023	[132]				

3.1. CFD analysis of single-phase systems

CFD simulations provide a convenient procedure to examine and correlate changes in the micromixing process to the size and distribution

of the produced nanoparticles. In single-phase systems polymeric nanoparticles are typically produced by nanoprecipitation, which is governed by mutual solvent diffusion and the transport of solute molecules from the organic phase toward the interface [30]. Accordingly, CFD simulations must resolve mass transfer and solvent diffusion to capture the physicochemical drivers of particle formation. By contrast, lipid-based nanoparticles are formed by self-assembly, where rapid mixing of amphiphilic molecules leads to spontaneous organisation into stable bilayer vesicular structures [31]. Indications of how rapidly the molecules diffuse can be provided through mass fraction profiles along the microchannels, revealing optimum conditions in which mixing occurs [93]. So far, CFD has enabled the quantification of mixing dynamics e.g., velocity and shear stress profiles, mixing time, mass transfer between fluids, and detailed analysis of mixing conditions. Additionally, it has revealed improved mixing grades in configurations that induce secondary flows, such as curved channels or channels with multiple inlets [104]. Therefore, researchers have used this information to associate different operating conditions with the size of nanoparticles obtained, based on the degree of mixing achieved [96]. In the case of inorganic nanoparticles, such as gold or silica, precipitation or reduction reactions within microdevices dominate. Consequently, CFD simulations must be coupled with reaction kinetics and PBM to capture nucleation, growth, and Ostwald ripening dynamics [31].

3.1.1. Hydrodynamic control of nanoparticle formation

Typically, the control of the formation of nanoparticles is done by changing the growth conditions. This is feasible through changes in the micromixer geometry and by the adjustment of the mixing time. CFD has provided useful information on their effects on nanoparticle nucleation and growth. Kimura et al. (2021) suggested the creation of 3D secondary flows in iLiNP devices, to achieve homogenous and slow rate solvent dilution [125]. Using CFD simulations, they analysed the solvent dilution in both 2D and 3D devices (Fig. 7A) and revealed that secondary flows only appear in the 3D device, which provides preferable dilution conditions to enable control of the nanoparticles' size. Similarly, Kim et al. [128] attempted to control the microvortices generated during

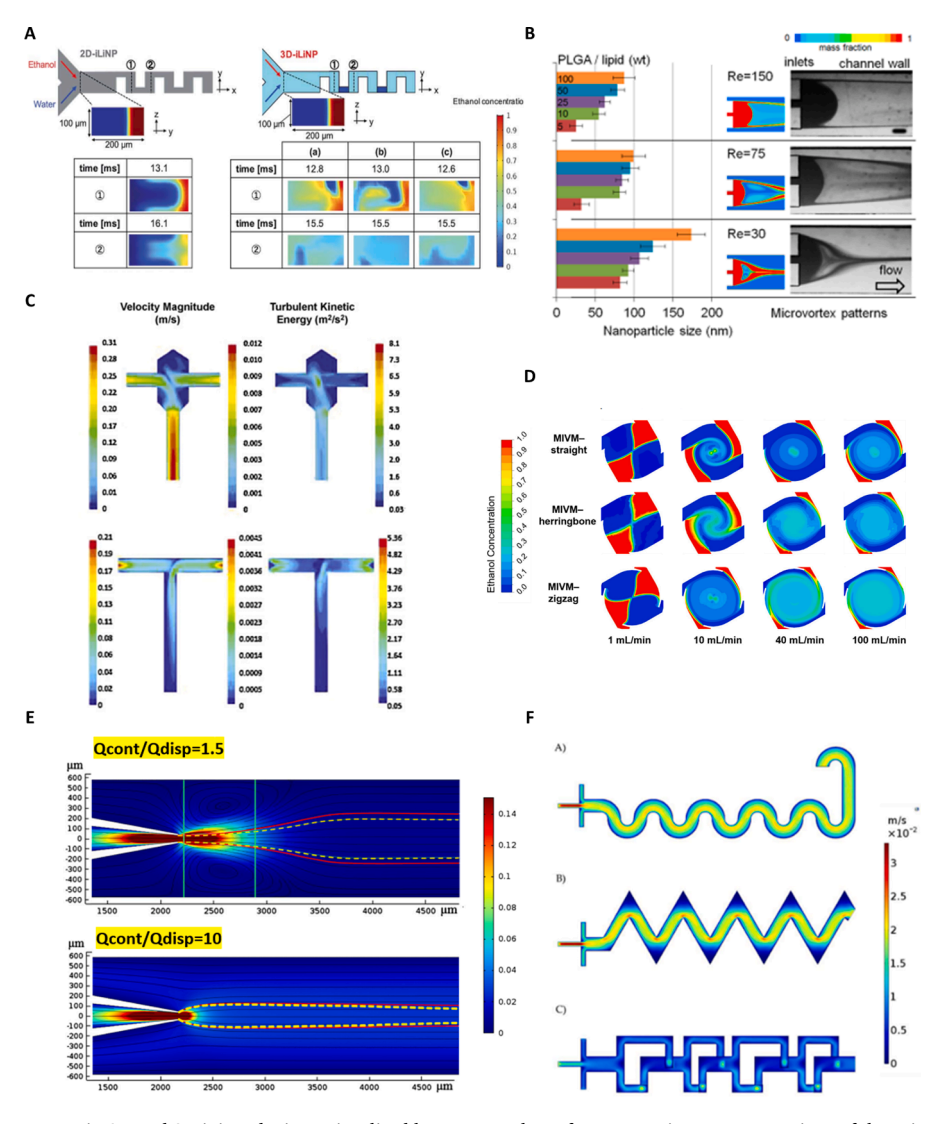


Fig. 7. (A) Ethanol dilution process in 2D and 3D iLiNP devices, visualised by contour plots of concentration at cross sections of the Y-junction at different moments. Colours represent the concentration of ethanol and the blue shows that the mass fraction of ethanol is zero [125], (B) Microvortex patterns in 3D flow focusing device for diverse Reynolds numbers obtained from both CFD and microscopic images along with the respective nanoparticle sizes produced [128], (C) Contour plots of velocity magnitude and turbulent kinetic energy from CFD results, in a CIJR (top) and Tee-mixer (bottom) for R = 1 and aqueous phase flow rate 20 ml/min [104], (D) Comparison of mixing efficiency in three types of Multi-vortex mixers through contour plots of solvent mass fraction (Flow rate ratio of the continuous to dispersed phase is equal to 3) [66], (E) Distribution of velocity for different flow rate ratios in a co-flow microfluidic device. The black lines are the streamlines, the red and yellow lines represent the areas of nanoparticles' nucleation and growth composed of two different types of polymers [30], (F) Contour plots of velocity profiles in three different types of micromixers used for magnetite nanoparticle synthesis [94].

nanoparticle growth by changing the flow rates, to obtain uniform-sized NPs [128]. They revealed that the formation of NPs relies on well-developed microvortices. Insufficient inertial forces, which are characterised by low Reynolds Numbers (Re=30), lead to underdeveloped microvortex (Fig. 7B). This causes insufficient mixing, wide nanoparticle size distribution, and larger particle sizes, explained by polymer aggregation. Based on the assumption that better mixing conditions induce the formation of smaller particles, Lince F. et al. (2011), compared the efficiency of a confined impinging jet reactor (CIJR) and a T-mixer [104]. They developed contour plots of velocity magnitude, turbulent kinetic energy, turbulent intensity, mean mixture fraction, and mixture fraction variance (Fig. 7C), and they showed that CIJRs are more efficient in converting the pressure drop into turbulence, resulting in smaller-sized particles. On the contrary, Zheng et al. [66], recently suggested that even though different degrees of mixing were achieved in three microvortex mixers with different inlet geometries, it had no significant impact on the final product size and distribution [66]. During their study, they used planar concentration contour plots within the mixing devices for various total flow rates (Fig. 7D) and reported that even though, in all the mixers, the efficiency increased with increasing total flow rate, a zigzag geometry performed better than a straight and herringbone configuration. It has been also observed that channels with higher surface-to-volume ratio (smaller diameter) have better heat transfer rates [117]. The rapid mass and heat transfer rates lead to improved mixing efficiency, allowing the generation of narrower size distribution. However, a larger surface-to-volume ratio can lead to stronger interfacial effects between the wall and the fluids, which results in larger particle size and wider distribution of the nanoparticles [117].

3.1.2. Effect of microfluidic mixing on particle nucleation and growth

Planar concentration profiles and plots of velocity fields allow spatial resolution of the fluid's distribution and homogenization. Fluid flow patterns can be evaluated and provide a qualitative reference of the location or the incremental volume in a microchannel, in which nucleation occurs [68,83,119]. Capretto et al. [93] analysed the correlation between the process hydrodynamics and the formation of polymeric micelles [93]. Having detected experimentally the critical concentration of a solvent at which nanoparticles start to form, they ran CFD simulations to find the exact positions where this occurs. This was possible by obtaining mass fraction profiles along the simulated microchannels which reveal the solutions' compositions during the mixing process. They revealed that larger nanoparticles can be formed with an increase in either mixing time or polymer initial concentration, which results to slower diffusion and mixing. In their subsequent work, they revealed some interesting findings on the distinction of two regions on flow focusing devices [118]. The first region located at the channel junction was described by rapid convective-diffusive mixing, whilst the second region was observed downstream of the channel junction, which showed limited mixing due to the molecular diffusion in the direction normal to the streamlines. These findings were further analyzed by Jaouhari et al. (2020), who employed coupled CFD and PBM simulations to investigate the nucleation and growth of organic nanoparticles under turbulent conditions in microreactors. Their study demonstrated that reducing the mixing time by decreasing the fluid flow rates, can lead to insufficient mixing, which, in turn, can influence the degree of supersaturation and favor particle growth over nucleation leading to broader particle size distributions [112]. Similarly, Othman et al. (2015) performed a 3D CFD analysis to obtain concentration profiles and identify the regions, where nanoparticles begin to form based on the solubility of polymers in the aqueous phase [30]. Their simulations revealed that variations in flow rate ratio between the two phases significantly affect these nucleation zones (Fig. 7E). At lower flow rate ratios, the formation of vortices was observed, which can trap particles and impact their residence time and growth. These findings align with the observations of Casado et al. (2024), who reported that at low mixing rates, induced by high flow rate ratios, particle synthesis occurs in a small volume at the fluids' interface

[105]. In contrast, at higher mixing rates, mixing is more homogeneous and nucleation occurs throughout the entire reaction volume, leading to the formation of particles with smaller sizes. Significant information about the behaviour of the nanoparticles formed inside a microchannel can be also provided through velocity and shear rate profiles [133]. Recently, Florez et al. (2022) applied this methodology and revealed areas of dead volume along sharp corners that cause nanoparticle accumulation in both 2D and 3D micromixer configurations (Fig. 7F), which resulted in inefficient mixing of reagents for the 2D devices. Although areas of dead volume also appeared in the 3D design, changes in the flow direction promoted the interaction between the reacting species, while the shear rate values were higher than the 2D devices, leading to smaller particle sizes with narrow size distribution [94].

3.2. CFD analysis of multiphase systems

Multiphase systems have received increased attention for nanoparticle synthesis, as a promising alternative to improve the performance of single-phase systems [97]. Amongst the flow patterns generated from the interaction of immiscible fluids (annular flow, slug flow, droplet flow), droplet flow is mostly desired to increase the interfacial area and the mixing efficiency inside the droplet and produce uniform particles [97]. Recently, CFD simulations have been conducted to provide a better understanding of the droplet breakup mechanism and the physicochemical parameters that affect their size and shape [134]. Attempts have also been made to create predictive models of the droplet length and generation rate [135]. Some of the most common methodologies applied include the modelling of surface tension, the study of pressure and velocity profiles near the interface of the two phases, and the investigation of the internal motion of the droplets [129]. Although droplet formation mechanism in microfluidic conditions has been extensively studied, both numerically and experimentally, there is limited understanding of how droplet characteristics affect the properties of the obtained nanoparticles.

3.2.1. Droplet formation mechanisms

One of the most used mixing configurations in microfluidics is the Tjunction structure, where the droplets can form into three regimes of flow: 1) Squeezing, 2) Dripping and 3) Jetting (Fig. 8A). During the squeezing regime, which is characterized by low Capillary numbers (describing the competition between viscous stresses, acting to elongate the interface, and surface tension attempting to minimize the surface area), the shear force created by the continuous phase is much smaller than the interfacial force. In this case, the dispersed phase gradually moves through the microfluidic junction and almost completely blocks the junction outlet, which leads to increased pressure and subsequent droplet formation. In the dripping regime, the shear force overcomes the interfacial tension, with the Ca number being high enough, and the droplet breaks up before the dispersed phase blocks the channel [95]. At even higher flow rates of the dispersed and continuous phases, where the Ca number is further increased, a liquid jet is formed, and the droplet breakup occurs far from the impingement point in the downstream of the channel [71,136]. Another configuration used for the formation of droplets is the co-axial flow devices (Fig. 3F); within this configuration viscous stresses that are created when the two phases come in contact cause the interface to stretch and finally break to form droplets [137]. In this case, the droplet generation is observed in the dripping or jetting regime. In flow focusing designs, the break-up of the droplet is achieved by squeezing the dispersed phase into a narrow stream surrounded by the continuous phase, providing the most stable emulsions, due to the symmetrical shearing [137]. The droplet formation in these channels is characterized by squeezing, dripping, or jetting regimes, while it has been observed numerically that decreasing the interfacial tension results in transition from dripping to jetting regime (Fig. 8B) [134].

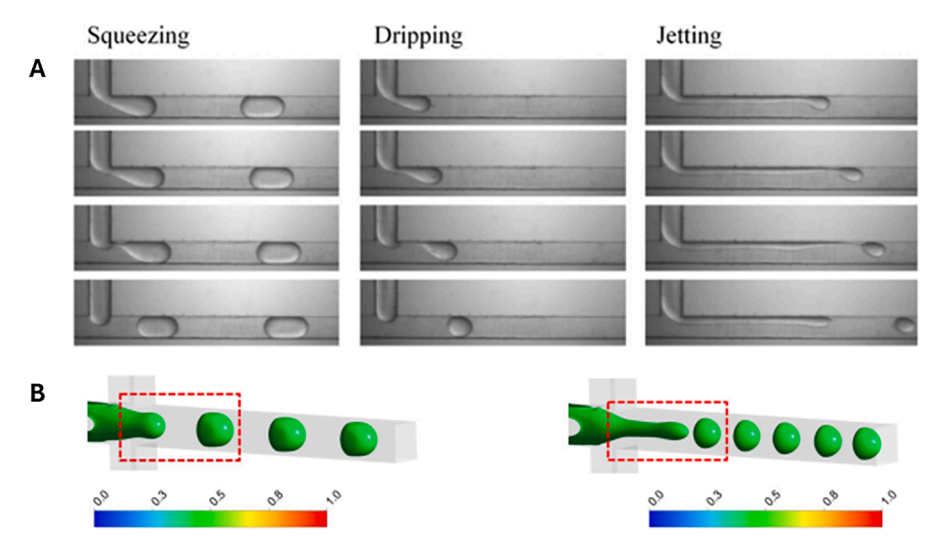


Fig. 8. (A) Micrographs of droplet formation in different regimes using a microfluidic T-junction [138], (B) CFD images of droplet formation in microfluidic flow focusing device on the dripping (left) and jetting (right) regime for Ca numbers of 0.025 and 0.041 respectively. The flow rate ratio of the continuous to the dispersed phase was constant and equal to 2 with the flow rate of continuous phase being 400 μL/min [134].

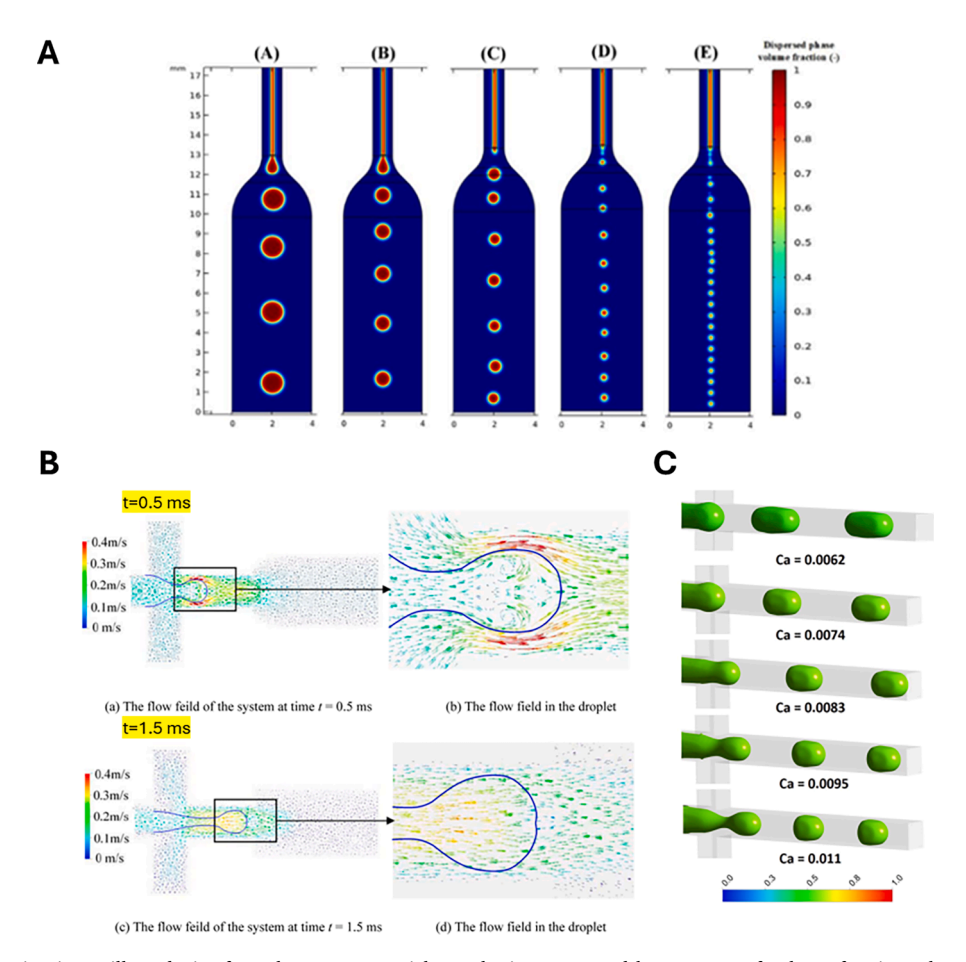


Fig. 9. (A) Droplet formation in capillary device for polymer nanoparticle synthesis represented by contours of volume fraction. The red colours show that the volume fraction of the dispersed phase is equal to 1 and the blue that it is equal to 0. The velocity of the dispersed phase is constant at 0.001 m/s and the velocity of the continuous phase is a)0.05 m/s, b) 0.1 m/s, c) 0.15 m/s, d) 0.2 m/s and e) 0.3 m/s [129], (B) CFD results of the velocity field during droplet formation in flow focusing structure for velocities of continuous and dispersed phase equal to 0.132 m/s and 0.04 m/s respectively [143], (C) CFD images showing the effect of interfacial tension, expressed by Capillary number, on the droplet shape. The flow rate ratio of the continuous to the dispersed phase was constant and equal to 2 with the flow rate of continuous phase being 400 μ L/min [134].

3.2.2. Numerical simulations of droplet formation

Numerical simulations can help to increase our understanding of the droplet formation mechanisms, revealing local information about pressure and shear forces competing with interfacial tension during the formation stage. CFD results have been reported to provide more accurate estimations of droplet size than existing theoretical models, allowing the development of surrogate models for the prediction of droplet characteristics by performing CFD simulations [129,135]. Analysis of CFD simulations allows the determination of the effect of various geometrical and physicochemical parameters on the final droplet features, including the droplet generation rate and size [127]. For instance, Bariki et al. (2022), used contours of volume fraction to quantify the effect of the dispersed and continuous phase flow rate on the droplet size and developed a numerical model for accurate estimation of droplet size in terms of the capillary numbers of the two phases (Fig. 9A) [129]. They reported that by increasing continuous phase velocity, the droplet size decreases due to the increasing shear force overcoming the interfacial force, and more fine particles are produced. During simulations of droplet generation, results have shown that the more viscous fluid (dispersed phase) is detached from the walls and is pulled by the less viscous fluid (continuous phase) increasing the surface-to-volume ratio of the contact interface. As a result, fast mixing and high shear stress occur, leading to smaller and less polydisperse nanoparticles [96].

3.2.3. From microfluidic droplet to particle formation

Nanoparticle size has been associated with the formation and manipulation of droplets that act as independent microreactors for nanoparticle production [42]. During emulsification, particles start to form after the organic solvent of the dispersed phase diffuses in the antisolvent of the continuous phase, reaching supersaturated condition inside the droplet as the concentration of the dissolved material increases. In that case, the residence time of the droplet, from the formation to the outlet of the channel, is considered as the overall duration of the precipitation process [83]. Thus, it is important to reveal complex flow patterns and mixing phenomena inside the droplets to get information about nanoparticle growth. Some investigations have used optical experimental techniques, such as Particle Image Velocimetry (PIV), to reveal these patterns [139-141]. However, these techniques face many limitations, such as difficulties in discriminating the two phases, and deflection of the light rays [142]. As a result, CFD simulations have been performed to examine multiphase flows. Lan et al. (2014) simulated the droplet formation in a flow focusing geometry and they reported that in the early stages of the formation, there is strong circulation inside the droplet, because of the shear stress associated with the flow rate of the continuous phase. However, at the later stage there was no circulation and the velocity of the droplet significantly increased (Fig. 9B) [100]. Recirculation phenomena inside the droplets can be controlled through adjustments in the fluids' properties and velocities. For example, Sontti et al. (2020) reported that an increase in continuous phase viscosity causes an increase in the velocity magnitude inside the droplet [134]. They also described changes in the droplet shape for different values of Ca number. They found that when the Ca is increased by increasing the flow rates, the droplet shape changes from plug to near spherical (Fig. 9C). However, Ježková et al. (2022) claimed that, even though the reduction of the droplets' size and the distance between them are important parameters for NP growth, the high pressure created by increasing the flow rates increases the mechanical stress acting on the assembling nanoparticles and should be considered [130].

3.2.4. Two reagent droplet formation: mixing inside droplets

Apart from providing a homogenous environment for nanoparticle nucleation and growth, droplets can be used as microreactors, allowing the controllable mixing of two or more reagents inside them for nanoparticle fabrication. Benyahia et al. (2021) used a capillary device and showed that improved mixing efficiency inside the droplets results in

smaller mean particle size [124]. The mixing efficiency was quantified by calculating differences in the local concentration of a material at a specific time, over the whole droplet surface area, from the initial and final (in case of fully mixed streams) concentration. They proved numerically that smaller droplets offer better mixing, due to improved chaotic advection in a smaller volume of fluid [124]. Furthermore, the numerical model revealed a recirculation area at the wall of the injection capillary orifice tip, which affects the reaction rate and yield (Fig. 10A). This is attributed to changes in the residence time of the reagents and a degree of premixing achieved. For instance, low flow rates of dispersed phase result in low velocities in the recirculation area and bigger droplets. Thus, the residence time of one of the streams is increased and the mixing efficiency is poor, resulting in larger particles. Kaspar et al. (2019) made a similar observation, claiming that these recirculation areas accelerate the homogenization of the reagents prior to droplet formation [122]. In their subsequent work, after having characterized the mixing process inside the droplet along the chosen microchannel (Fig. 10B), they investigated the effect of the channel height on the synthesis of nanoparticles [83]. They observed that increasing channel height can produce larger droplets, however, the nanoparticles produced are more uniform (Fig. 10C). This was explained by the longer premixing period [83].

4. Future perspective

Most microfluidic-assisted drug delivery systems are at pre-clinical stage, and they require further investigations. Advanced drug delivery systems require careful design and optimization of existing and novel microfluidic platforms, including several steps for efficient nanoformulation. For example, multi-step, automated microfluidic designs, integrating real-time characterization techniques need to be developed. These techniques, such as dynamic light scattering (DLS) allow direct monitoring of any change in the nanoparticle formation by optimizing the microfluidic parameters [10]. Furthermore, automated systems need to be integrated in microfluidic platforms to provide rapid screening of nanoparticles and allow optimization without redesigning the process.

Adoption of CFD simulations could be beneficial to predict nanoparticle properties by reducing the experimental cost and allowing the redesign and optimization of several microfluidic configurations. For example, the geometries of co-axial capillary devices (tip diameters, distance between capillaries, shape of the tips) can be further investigated to provide optimum hydrodynamic conditions and generate uniform nanoparticles of specific size [124]. Insight should be given on the nanoparticle production via emulsification to fully characterize mixing phenomena inside the droplets and their stability. A better understanding of the effect of various process parameters (pressure, temperature, flow rate ratio, concentration) through CFD analysis can lead to the development of surrogate models, which predict nanoparticle characteristics and enable the selection of optimum parameters for the formation of the desired product.

5. Conclusions

Recent progress in the fabrication of complex microfluidic systems has enabled the preparation of multifunctional nanoparticles with uniform size and morphology for advanced drug delivery applications. Optimizing production process can provide better control of nanoparticles with desired properties and increased encapsulation efficiency of bioactive molecules. Considering the benefits of microfluidics in drug delivery applications, the existing microfluidic devices and methods used for nanoparticle synthesis are reported. While passive devices dominate current practice, active mixers incorporating acoustic, electrokinetic, and pneumatic actuation offer powerful means to tune NP properties. CFD modelling offers a powerful tool for optimizing microfluidic devices, ensuring efficient nanoparticle synthesis. The importance of CFD analysis is depicted by reporting recent observations in

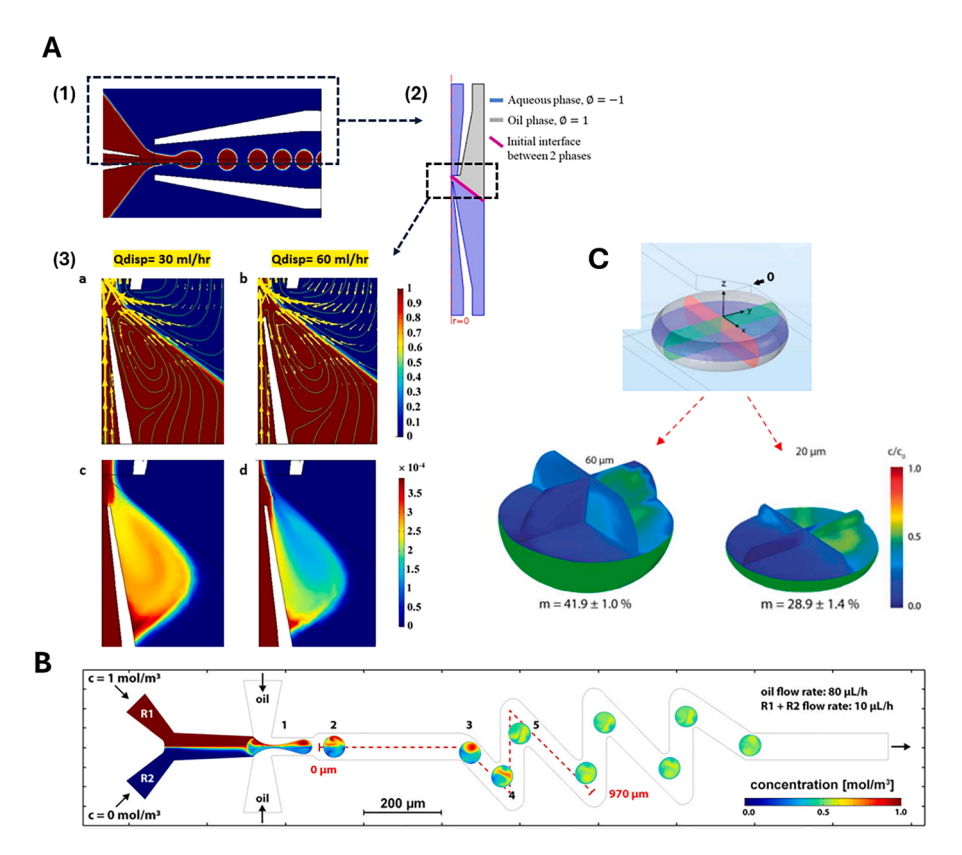


Fig. 10. (A) 1) Capillary device with contours of phase fraction 2) Initial conditions applied in the CFD study 3) Contours of velocity fields (a-b) obtained from CFD analysis showing recirculation areas generated in droplet microfluidic capillary device for different values of dispersed phase flow rate. The colours represent the mass fraction of the continuous phase. Images c-d show the distribution of the concentration of the material used to prepare nanoparticles in the respective recirculation areas [124],(B) Mixing efficiency achieved inside the droplets generated in microfluidic X-junction channel revealed by contour plots of the solvents mass fraction in cross sectional areas along the microchannel [122], (C) CFD analysis of solvent distribution inside droplets generated by different channel heights (60 & 40 μ m). The areas of interest are perpendicular planes inside the droplet, which is tangent to the reference point 0 [83].

mixing phenomena and droplet generation in microchannels, as they can provide significant insight on the fluidic environment during nanoparticle formation. When coupled with PBMs, this approach enables thorough understanding and predictive capability of nanoparticle nucleation and growth, thereby leading to optimal design of geometry and process parameters of the microfluidic system. Beyond drug delivery, the CFD approaches discussed here are broadly applicable to other nanoparticle domains such as environmental remediation, and their integration with experimental validation is expected to be pivotal in addressing scale-up challenges for industrial translation.

Funding information

The authors gratefully acknowledge funding from EPSRC (Grant No. EP/W027461/1).

CRediT authorship contribution statement

Anna Tsitouridou: Writing – original draft, Formal analysis, Conceptualization, Investigation, Methodology. Maryam Parhizkar: Writing – review & editing, Supervision, Conceptualization. Chuan-Yu Wu: Writing – review & editing, Supervision, Conceptualization. Tao Chen: Writing – review & editing, Supervision, Conceptualization. Dimitrios Tsaoulidis: Writing – review & editing, Supervision, Conceptualization, Methodology, Resources.

Declaration of competing interest

The authors declare that they have no known competing financial

interests or personal relationships that could have appeared to influence the work reported in this paper.

Acknowledgements

The authors gratefully acknowledge funding from EPSRC (Grant No. EP/W027461/1). Anna Tsitouridou also acknowledges the University of Surrey for the provision of a doctoral scholarship. For open access, the authors have applied a Creative Commons attribution license (CC BY) to any Author Accepted Manuscript version arising from this submission.

Data availability

No data was used for the research described in the article.

References

- [1] C.J. Martínez Rivas, M. Tarhini, W. Badri, K. Miladi, H. Greige-Gerges, Q. A. Nazari, S.A. Galindo Rodríguez, R.Á. Román, H. Fessi, A. Elaissari, Nanoprecipitation process: from encapsulation to drug delivery, Int. J. Pharm. 532 (2017) 66–81, https://doi.org/10.1016/j.ijpharm.2017.08.064.
- [2] M. Parhizkar, D. Tsaoulidis, The outlook for novel pharmaceutics, in: P. Zhu, L. Wang, Microfluidics-Enabled Soft Manufacture, Springer International Publishing, Cham, 2022: pp. 301–315. https://doi.org/10.1007/978-3-030-99838-7 16.
- [3] X. Shan, X. Gong, J. Li, J. Wen, Y. Li, Z. Zhang, Current approaches of nanomedicines in the market and various stage of clinical translation, Acta Pharm. Sin. B 12 (2022) 3028–3048, https://doi.org/10.1016/j. apsb.2022.02.025.
- [4] C. Lopes, J. Cristóvão, V. Silvério, P.R. Lino, P. Fonte, Microfluidic production of mRNA-loaded lipid nanoparticles for vaccine applications, Expert Opin. Drug Deliv. 19 (2022) 1381–1395, https://doi.org/10.1080/17425247.2022.2135502.

- [5] M.J. Mitchell, M.M. Billingsley, R.M. Haley, M.E. Wechsler, N.A. Peppas, R. Langer, Engineering precision nanoparticles for drug delivery, Nat. Rev. Drug Discov. 20 (2021) 101–124, https://doi.org/10.1038/s41573-020-0090-8.
- [6] E. Musielak, A. Feliczak-Guzik, I. Nowak, Synthesis and potential applications of lipid nanoparticles in medicine, Materials 15 (2022), https://doi.org/10.3390/ ma15020682
- [7] A. Zielinska, F. Carreiró, A.M. Oliveira, A. Neves, B. Pires, D. Nagasamy Venkatesh, A. Durazzo, M. Lucarini, P. Eder, A.M. Silva, A. Santini, E.B. Souto, Polymeric nanoparticles: production, characterization, toxicology and ecotoxicology, Molecules 25 (2020), https://doi.org/10.3390/ molecules25163731.
- [8] S. Tiwari, G. Yadav, S. Sharma, P. Srivastava, A. Kumar, Inorganic nanoparticles: a review on method and material for fabrication, Ind. J. Pharm. Pharmacol. 9 (2022) 158–163, https://doi.org/10.18231/j.ijpp.2022.028.
- [9] N.T.K. Thanh, N. Maclean, S. Mahiddine, Mechanisms of nucleation and growth of nanoparticles in solution, Chem. Rev. 114 (2014) 7610–7630, https://doi.org/ 10.1021/cr400544s
- [10] M.A. Tomeh, X. Zhao, Recent advances in microfluidics for the preparation of drug and gene delivery systems, Mol. Pharm. 17 (2020) 4421–4434, https://doi. org/10.1021/acs.molpharmaceut.0c00913.
- [11] K.J. Wu, E.C.M. Tse, C. Shang, Z. Guo, Nucleation and growth in solution synthesis of nanostructures - from fundamentals to advanced applications, Prog. Mater. Sci. 123 (2022), https://doi.org/10.1016/j.pmatsci.2021.100821.
- [12] X.T. Sun, M. Liu, Z.R. Xu, Microfluidic fabrication of multifunctional particles and their analytical applications, Talanta 121 (2014) 163–177, https://doi.org/ 10.1016/j.talanta.2013.12.060.
- [13] Z. Liu, F. Fontana, A. Python, J.T. Hirvonen, H.A. Santos, Microfluidics for production of particles: mechanism, methodology, and applications, Small 16 (2020), https://doi.org/10.1002/smll.201904673.
- [14] Q. Ma, J. Cao, Y. Gao, S. Han, Y. Liang, T. Zhang, X. Wang, Y. Sun, Microfluidic-mediated nano-drug delivery systems: from fundamentals to fabrication for advanced therapeutic applications, Nanoscale 12 (2020) 15512–15527, https://doi.org/10.1039/d0m/02397c.
- [15] F. Ejeta, Recent advances of microfluidic platforms for controlled drug delivery in nanomedicine, Drug Des. Devel. Ther. 15 (2021) 3881–3891, https://doi.org/ 10.2147/DDDT.S324580.
- [16] K. Amreen, S. Goel, Review—miniaturized and microfluidic devices for automated nanoparticle synthesis, ECS J. Solid State Sci. Technol. 10 (2021) 017002, https://doi.org/10.1149/2162-8777/abdb19.
- [17] S.J. Shepherd, D. Issadore, M.J. Mitchell, Microfluidic formulation of nanoparticles for biomedical applications, Biomaterials 274 (2021), https://doi. org/10.1016/j.biomaterials.2021.120826.
- [18] L. Zhang, Q. Chen, Y. Ma, J. Sun, Microfluidic methods for fabrication and engineering of nanoparticle drug delivery systems, ACS Appl. Bio Mater. 3 (2020) 107–120, https://doi.org/10.1021/acsabm.9b00853.
- [19] Z. Ma, B. Li, J. Peng, D. Gao, Recent development of drug delivery systems through microfluidics: from synthesis to evaluation, Pharmaceutics 14 (2022), https://doi.org/10.3390/pharmaceutics14020434
- [20] F. Tian, L. Cai, C. Liu, J. Sun, Microfluidic technologies for nanoparticle formation, Lab Chip 22 (2022) 512–529, https://doi.org/10.1039/d1lc00812a.
- [21] L. Zhang, J. Sun, Microfluidics for nanomaterial synthesis. Multidisciplinary Microfluidic and Nanofluidic Lab-on-a-Chip: Principles and Applications, Elsevier, 2021, pp. 429–453, https://doi.org/10.1016/B978-0-444-59432-7.00015-7.
- [22] A. Maged, R. Abdelbaset, A.A. Mahmoud, N.A. Elkasabgy, Merits and advances of microfluidics in the pharmaceutical field: design technologies and future prospects, Drug Deliv. 29 (2022) 1549–1570, https://doi.org/10.1080/ 10717544.2022.2069878.
- [23] C.T. Kung, H. Gao, C.Y. Lee, Y.N. Wang, W. Dong, C.H. Ko, G. Wang, L.M. Fu, Microfluidic synthesis control technology and its application in drug delivery, bioimaging, biosensing, environmental analysis and cell analysis, Chem. Eng. J. 399 (2020), https://doi.org/10.1016/j.cej.2020.125748.
- [24] D. Liu, H. Zhang, F. Fontana, J.T. Hirvonen, H.A. Santos, Current developments and applications of microfluidic technology toward clinical translation of nanomedicines, Adv. Drug Deliv. Rev. 128 (2018) 54–83, https://doi.org/ 10.1016/j.addr.2017.08.003.
- [25] F. Jia, Y. Gao, H. Wang, Recent advances in drug delivery system fabricated by microfluidics for disease therapy, Bioengineering 9 (2022) 625, https://doi.org/ 10.3390/bioengineering9110625.
- [26] R. Riahi, A. Tamayol, S.A.M. Shaegh, A.M. Ghaemmaghami, M.R. Dokmeci, A. Khademshosseini, Microfluidics for advanced drug delivery systems, Curr. Opin. Chem. Eng. 7 (2015) 101–112, https://doi.org/10.1016/j. coche.2014.12.001.
- [27] D. Liu, H. Zhang, F. Fontana, J.T. Hirvonen, H.A. Santos, Microfluidic-assisted fabrication of carriers for controlled drug delivery, Lab Chip 17 (2017) 1856–1883, https://doi.org/10.1039/c7lc00242d.
- [28] J. Ahn, J. Ko, S. Lee, J. Yu, Y.T. Kim, N.L. Jeon, Microfluidics in nanoparticle drug delivery; from synthesis to pre-clinical screening, Adv. Drug Deliv. Rev. 128 (2018) 29–53, https://doi.org/10.1016/j.addr.2018.04.001.
- [29] A.G. Niculescu, D.E. Mihaiescu, A.M. Grumezescu, A review of microfluidic experimental designs for nanoparticle synthesis, Int. J. Mol. Sci. 23 (2022), https://doi.org/10.3390/ijms23158293.
- [30] R. Othman, G.T. Vladisavljević, H.C. Hemaka Bandulasena, Z.K. Nagy, Production of polymeric nanoparticles by micromixing in a co-flow microfluidic glass capillary device, Chem. Eng. J. 280 (2015) 316–329, https://doi.org/10.1016/j. cej.2015.05.083.

- [31] A. Agha, W. Waheed, I. Stiharu, V. Nerguizian, G. Destgeer, E. Abu-Nada, A. Alazzam, A review on microfluidic-assisted nanoparticle synthesis, and their applications using multiscale simulation methods, Discov. Nano 18 (2023), https://doi.org/10.1186/s11671-023-03792-x.
- [32] P. Zhao, J. Wang, C. Chen, J. Wang, G. Liu, K. Nandakumar, Y. Li, L. Wang, Microfluidic applications in drug development: fabrication of drug carriers and drug toxicity screening, Micromachines 13 (2022), https://doi.org/10.3390/ mil.3020200
- [33] I. Lignos, R. Maceiczyk, A.J. DeMello, Microfluidic technology: uncovering the mechanisms of nanocrystal nucleation and growth, Acc. Chem. Res. 50 (2017) 1248–1257, https://doi.org/10.1021/acs.accounts.7b00088.
- [34] Z. Liu, F. Fontana, A. Python, J.T. Hirvonen, H.A. Santos, Microfluidics for production of particles: mechanism, methodology, and applications, Small 16 (2020), https://doi.org/10.1002/smll.201904673.
- [35] A. Gerami, Y. Alzahid, P. Mostaghimi, N. Kashaninejad, F. Kazemifar, T. Amirian, N. Mosavat, M.E. Warkiani, R.T. Armstrong, Microfluidics for porous systems: fabrication, microscopy and applications, Transp. Porous Med. 130 (2019) 277–304, https://doi.org/10.1007/s11242-018-1202-3.
- [36] Y. Zhu, Q. Fang, Analytical detection techniques for droplet microfluidics-a review, Anal. Chim. Acta 787 (2013) 24–35, https://doi.org/10.1016/j. aca.2013.04.064.
- [37] P. Zhou, H. He, H. Ma, S. Wang, S. Hu, A review of optical imaging technologies for microfluidics, Micromachines 13 (2022), https://doi.org/10.3390/ mi13020274.
- [38] L.Y. Chu, A.S. Utada, R.K. Shah, J.W. Kim, D.A. Weitz, Controllable monodisperse multiple emulsions, Angew. Chem. - Int. Ed. 46 (2007) 8970–8974, https://doi. org/10.1002/anie.200701358.
- [39] P. Angeli, D. Tsaoulidis, W. Hashi Weheliye, Studies on mass transfer of europium (III)in micro-channels using a micro laser induced fluorescence technique, Chem. Eng. J. 372 (2019) 1154–1163, https://doi.org/10.1016/j.cej.2019.04.084.
- [40] F. Shen, Y. Li, Z. Liu, X.J. Li, Study of flow behaviors of droplet merging and splitting in microchannels using Micro-PIV measurement, Microfluid. Nanofluid. 21 (2017), https://doi.org/10.1007/s10404-017-1902-y.
- [41] S.K. Luther, S. Will, A. Braeuer, Phase-specific Raman spectroscopy for fast segmented microfluidic flows, Lab Chip 14 (2014) 2910–2913, https://doi.org/ 10.1030/c4lc00428k
- [42] J. Ma, S.M.Y. Lee, C. Yi, C.W. Li, Controllable synthesis of functional nanoparticles by microfluidic platforms for biomedical applications-a review, Lab Chip 17 (2017) 209–226, https://doi.org/10.1039/C6LC01049K.
- [43] D.J. Kang, Effects of baffle configuration on mixing in a T-shaped micro-channel, Micromachines 6 (2015) 765–777, https://doi.org/10.3390/mi6060765.
- [44] D. Liu, S. Cito, Y. Zhang, C.F. Wang, T.M. Sikanen, H.A. Santos, A versatile and robust microfluidic platform toward high throughput synthesis of homogeneous nanoparticles with tunable properties, Adv. Mater. 27 (2015) 2298–2304, https://doi.org/10.1002/adma.201405408.
- [45] Y. Matsuura-Sawada, M. Maeki, T. Nishioka, A. Niwa, J. Yamauchi, M. Mizoguchi, K. Wada, M. Tokeshi, Microfluidic device-enabled mass production of lipid-based nanoparticles for applications in nanomedicine and cosmetics, ACS Appl. Nano Mater. (2022), https://doi.org/10.1021/acsanm.2c00886.
 [46] M. Maeki, Y. Okada, S. Uno, A. Niwa, A. Ishida, H. Tani, M. Tokeshi, Production
- [46] M. Maeki, Y. Okada, S. Uno, A. Niwa, A. Ishida, H. Tani, M. Tokeshi, Production of siRNA-loaded lipid nanoparticles using a microfluidic device, J. Visualiz. Exp. 2022 (2022), https://doi.org/10.3791/62999.
- [47] K. Okuda, Y. Sato, K. Iwakawa, K. Sasaki, N. Okabe, M. Maeki, M. Tokeshi, H. Harashima, On the size-regulation of RNA-loaded lipid nanoparticles synthesized by microfluidic device, J. Controll. Rel. 348 (2022) 648–659, https://doi.org/10.1016/j.jconrel.2022.06.017.
- [48] C.E. Torres, J. Cifuentes, S.C. Gómez, V. Quezada, K.A. Giraldo, P.R. Puentes, L. Rueda-Gensini, J.A. Serna, C. Muñoz-Camargo, L.H. Reyes, J.F. Osma, J. C. Cruz, Microfluidic synthesis and purification of magnetoliposomes for potential applications in the gastrointestinal delivery of difficult-to-transport drugs, Pharmaceutics 14 (2022), https://doi.org/10.3390/ pharmaceutics14020315.
- [49] M. Abad, G. Mendoza, L. Usón, M. Arruebo, M. Piñol, V. Sebastián, L. Oriol, Microfluidic synthesis of block copolymer micelles: application as drug nanocarriers and as photothermal transductors when loading Pd nanosheets, Macromol. Biosci. (2022), https://doi.org/10.1002/mabi.202100528.
- [50] M. Li, C. Liu, J. Yin, G. Liu, D. Chen, Single-step synthesis of highly tunable multifunctional nanoliposomes for synergistic cancer therapy, ACS Appl. Mater. Interf. (2022), https://doi.org/10.1021/acsami.2c00600.
- [51] S. Gimondi, R.L. Reis, H. Ferreira, N.M. Neves, Microfluidic-driven mixing of high molecular weight polymeric complexes for precise nanoparticle downsizing, Nanomedicine 43 (2022), https://doi.org/10.1016/j.nano.2022.102560.
- [52] X. Joseph, V. Akhil, A. Arathi, P.V. Mohanan, Microfluidic synthesis of gelatin nanoparticles conjugated with nitrogen-doped carbon dots and associated cellular response on A549 cells, Chem. Biol. Interact. 351 (2022), https://doi.org/ 10.1016/j.cbi.2021.109710.
- [53] L.R. Fonseca, T.P. Santos, A. Czaikoski, R.L. Cunha, Microfluidics-based production of chitosan-gellan nanocomplexes encapsulating caffeine, Food Res. Int. 151 (2022), https://doi.org/10.1016/j.foodres.2021.110885.
- [54] G. Prakash, A. Shokr, N. Willemen, S.M. Bashir, S.R. Shin, S. Hassan, Microfluidic fabrication of lipid nanoparticles for the delivery of nucleic acids, Adv. Drug Deliv. Rev. 184 (2022), https://doi.org/10.1016/j.addr.2022.114197.
- [55] R. Xu, M.A. Tomeh, S. Ye, P. Zhang, S. Lv, R. You, N. Wang, X. Zhao, Novel microfluidic swirl mixers for scalable formulation of curcumin loaded liposomes for cancer therapy, Int. J. Pharm. 622 (2022), https://doi.org/10.1016/j. ijpharm.2022.121857.

- [56] W. Fan, F. Zhao, M. Chen, J. Li, X. Guo, Accelerated and simplified synthesis of magnetic mesoporous nanoparticles in a continuous multistep microfluidic system, Chem. Eng. Process. - Process Intensific. 181 (2022) 109104, https://doi. org/10.1016/j.cep.2022.109104.
- [57] M.A. Tomeh, M.H. Mansor, R. Hadianamrei, W. Sun, X. Zhao, Optimization of large-scale manufacturing of biopolymeric and lipid nanoparticles using microfluidic swirl mixers, Int. J. Pharm. 620 (2022), https://doi.org/10.1016/j. iipharm.2022.121762.
- [58] I. Eş, A.A. Malfatti-Gasperini, L.G. de la Torre, The diffusion-driven microfluidic process to manufacture lipid-based nanotherapeutics with stealth properties for siRNA delivery, Colloids Surf. B Biointerf. 215 (2022), https://doi.org/10.1016/j. colsurfh 2022 112476
- [59] Q. Cai, V. Castagnola, L. Boselli, A. Moura, H. Lopez, W. Zhang, J.M. De Araújo, K. A. Dawson, A microfluidic approach for synthesis and kinetic profiling of branched gold nanostructures, Nanoscale Horiz. 7 (2022) 288–298, https://doi.org/10.1039/d1nh0054de.
- [60] M.A. Tomeh, R. Hadianamrei, D. Xu, S. Brown, X. Zhao, Peptide-functionalised magnetic silk nanoparticles produced by a swirl mixer for enhanced anticancer activity of ASC-J9, Colloids Surf. B Biointerf. 216 (2022), https://doi.org/ 10.1016/j.colsurfb.2022.112549.
- [61] Y. Jin, T. Wang, Q. Li, F. Wang, J. Li, A microfluidic approach for rapid and continuous synthesis of glycoprotein-imprinted nanospheres, Talanta 239 (2022), https://doi.org/10.1016/j.talanta.2021.123084.
- [62] B. Küçüktürkmen, W. Inam, F. Howaili, M. Gouda, N. Prabhakar, H. Zhang, J. M. Rosenholm, Microfluidic-assisted fabrication of dual-coated pH-Sensitive mesoporous silica nanoparticles for protein delivery, Biosensors 12 (2022), https://doi.org/10.3390/bios12030181.
- [63] A. Giorello, A. Nicastro, C.L.A. Berli, Microfluidic platforms for the production of nanoparticles at flow rates larger than one liter per hour, Adv. Mater. Technol. (2022), https://doi.org/10.1002/admt.202101588.
- [64] N. Kimura, M. Maeki, Y. Sato, Y. Note, A. Ishida, H. Tani, H. Harashima, M. Tokeshi, Development of the iLiNP Device: fine tuning the lipid nanoparticle size within 10 nm for drug delivery, ACS Omega 3 (2018) 5044–5051, https:// doi.org/10.1021/acsomega.8b00341.
- [65] E. Chiesa, R. Dorati, T. Modena, B. Conti, I. Genta, Multivariate analysis for the optimization of microfluidics-assisted nanoprecipitation method intended for the loading of small hydrophilic drugs into PLGA nanoparticles, Int. J. Pharm. 536 (2018) 165–177, https://doi.org/10.1016/j.ijpharm.2017.11.044.
- [66] H. Zheng, H. Tao, J. Wan, K.Y. Lee, Z. Zheng, S.S.Y. Leung, Preparation of drug-loaded liposomes with multi-inlet vortex mixers, Pharmaceutics 14 (2022) 1223, https://doi.org/10.3390/pharmaceutics14061223.
- [67] S.J. Shepherd, C.C. Warzecha, S. Yadavali, R. El-Mayta, M.G. Alameh, L. Wang, D. Weissman, J.M. Wilson, D. Issadore, M.J. Mitchell, Scalable mRNA and siRNA lipid nanoparticle production using a parallelized microfluidic device, Nano Lett. 21 (2021) 5671–5680, https://doi.org/10.1021/acs.nanolett.1c01353.
 [68] D. Di, X. Qu, C. Liu, L. Fang, P. Quan, Continuous production of celecoxib
- [68] D. Di, X. Qu, C. Liu, L. Fang, P. Quan, Continuous production of celecoxib nanoparticles using a three-dimensional-coaxial-flow microfluidic platform, Int. J. Pharm. 572 (2019), https://doi.org/10.1016/j.ijpharm.2019.118831.
- [69] M. Parhizkar, D. Tsaoulidis, Emerging Drug Delivery and Biomedical Engineering Technologies: Transforming Therapy, Microfluidics for Drug Discovery and Development, 2023, p. 119.
- [70] C.T. Riche, E.J. Roberts, M. Gupta, R.L. Brutchey, N. Malmstadt, Flow invariant droplet formation for stable parallel microreactors, Nat. Commun. 7 (2016), https://doi.org/10.1038/ncomms10780.
- [71] S. Damiati, U.B. Kompella, S.A. Damiati, R. Kodzius, Microfluidic devices for drug delivery systems and drug screening, Genes 9 (2018), https://doi.org/10.3390/ genes9020103.
- [72] B.G. Carvalho, B.T. Ceccato, M. Michelon, S.W. Han, L.G. de la Torre, Advanced microfluidic technologies for lipid nano-microsystems from synthesis to biological application, Pharmaceutics 14 (2022) 141, https://doi.org/10.3390/ pharmaceutics14010141.
- [73] I.U. Khan, C.A. Serra, N. Anton, X. Li, R. Akasov, N. Messaddeq, I. Kraus, T. F. Vandamme, Microfluidic conceived drug loaded Janus particles in side-by-side capillaries device, Int. J. Pharm. 473 (2014) 239–249, https://doi.org/10.1016/j.iipharm.2014.06.035.
- [74] J.-W. Kim, S.H. Han, Y.H. Choi, W.M. Hamonangan, Y. Oh, S.-H. Kim, Recent advances in the microfluidic production of functional microcapsules by multipleemulsion templating, Lab Chip (2022), https://doi.org/10.1039/d2lc00196a.
- [75] M. Chen, R. Aluunmani, G. Bolognesi, G.T. Vladisavljević, Facile microfluidic fabrication of biocompatible hydrogel microspheres in a novel microfluidic device, Molecules 27 (2022) 4013, https://doi.org/10.3390/molecules27134013.
- [76] H. Nemoto, D. Shimba, T. Kanai, Preparation of monodisperse silicapolyacrylamide hybrid particles with snowman or core-shell morphologies using a microfluidic device, J. Asian Ceram. Soc. (2022), https://doi.org/10.1080/ 21870764.2022.2055858.
- [77] H.Q. Nguyen, T.S. Seo, A 3D printed size-tunable flow-focusing droplet microdevice to produce cell-laden hydrogel microspheres, Anal. Chim. Acta 1192 (2022), https://doi.org/10.1016/j.aca.2021.339344.
- [78] A. Larrea, M. Arruebo, C.A. Serra, V. Sebastián, Trojan pH-sensitive polymer particles produced in a continuous-flow capillary microfluidic device using waterin-oil-in-water double-emulsion droplets, Micromachines 13 (2022) 878, https:// doi.org/10.3390/mi13060878.
- [79] A.L.R. Costa, A. Gomes, R.L. Cunha, Studies of droplets formation regime and actual flow rate of liquid-liquid flows in flow-focusing microfluidic devices, Exp. Therm. Fluid Sci. 85 (2017) 167–175, https://doi.org/10.1016/j. expthermflusci.2017.03.003.

- [80] P. Zhu, L. Wang, Microfluidics-enabled soft manufacture of materials with tailorable wettability, Chem. Rev. 122 (2022) 7010–7060, https://doi.org/ 10.1021/acs.chemrev.1c00530.
- [81] J. Wang, Y. Li, X. Wang, J. Wang, H. Tian, P. Zhao, Y. Tian, Y. Gu, L. Wang, C. Wang, Droplet microfluidics for the production of microparticles and nanoparticles, Micromachines 8 (2017), https://doi.org/10.3390/mi8010022.
- [82] S.M. Giannitelli, E. Limiti, P. Mozetic, F. Pinelli, X. Han, F. Abbruzzese, F. Basoli, D. Del Rio, S. Scialla, F. Rossi, M. Trombetta, L. Rosanò, G. Gigli, Z.J. Zhang, E. Mauri, A. Rainer, Droplet-based microfluidic synthesis of nanogels for controlled drug delivery: tailoring nanomaterial properties via pneumatically actuated flow-focusing junction, Nanoscale 14 (2022) 11415–11428, https://doi.org/10.1039/DZNR00827K.
- [83] O. Kašpar, A.H. Koyuncu, A. Hubatová-Vacková, M. Balouch, V. Tokárová, Influence of channel height on mixing efficiency and synthesis of iron oxide nanoparticles using droplet-based microfluidics, RSC Adv. 10 (2020) 15179–15189, https://doi.org/10.1039/d0ra02470h.
- [84] L.H. Hung, S.Y. Teh, J. Jester, A.P. Lee, PLGA micro/nanosphere synthesis by droplet microfluidic solvent evaporation and extraction approaches, Lab Chip 10 (2010) 1820–1825, https://doi.org/10.1039/c002866e.
- [85] A.G. Niculescu, D.E. Mihaiescu, A.M. Grumezescu, A review of microfluidic experimental designs for nanoparticle synthesis, Int. J. Mol. Sci. 23 (2022), https://doi.org/10.3390/ijms23158293.
- [86] P.H. Huang, S. Zhao, H. Bachman, N. Nama, Z. Li, C. Chen, S. Yang, M. Wu, S. P. Zhang, T.J. Huang, Acoustofluidic synthesis of particulate nanomaterials, Adv. Sci. 6 (2019), https://doi.org/10.1002/advs.201900913.
- [87] A. Pourabed, J. Brenker, T. Younas, L. He, T. Alan, A Lotus shaped acoustofluidic mixer: high throughput homogenisation of liquids in 2 ms using hydrodynamically coupled resonators, Ultrason. Sonochem. 83 (2022), https://doi.org/10.1016/j.ultsonch.2022.105936.
- [88] P. Modarres, M. Tabrizian, Electrohydrodynamic-driven micromixing for the synthesis of highly monodisperse nanoscale liposomes, ACS Appl. Nano Mater. 3 (2020) 4000–4013, https://doi.org/10.1021/acsanm.9b02407.
- [89] X. Wang, X. Ma, L. An, X. Kong, Z. Xu, J. Wang, A pneumatic micromixer facilitating fluid mixing at a wide range flow rate for the preparation of quantum dots, Sci. China Chem. 56 (2013) 799–805, https://doi.org/10.1007/s11426-012-4808-2.
- [90] D. Liu, H. Zhang, S. Cito, J. Fan, E. Mäkilä, J. Salonen, J. Hirvonen, T.M. Sikanen, D.A. Weitz, H.A. Santos, Core/shell nanocomposites produced by superfast sequential microfluidic nanoprecipitation, Nano Lett. 17 (2017) 606–614, https://doi.org/10.1021/acs.nanolett.6b03251.
- [91] D. de O. Maionchi, L. Ainstein, F.P. dos Santos, M.B. de S Júnior, Computational fluid dynamics and machine learning as tools for optimization of micromixers geometry, (2022). http://arxiv.org/abs/2203.02498.
- [92] S. Rezvantalab, R. Maleki, N.I. Drude, M. Khedri, A. Jans, M. Keshavarz Moraveji, M. Darguzyte, E. Ghasemy, L. Tayebi, F. Kiessling, Experimental and computational study on the microfluidic control of micellar nanocarrier properties, ACS Omega 6 (2021) 23117–23128, https://doi.org/10.1021/ acsomega.102651.
- [93] L. Capretto, D. Carugo, W. Cheng, M. Hill, X. Zhang, Continuous-flow production of polymeric micelles in microreactors: experimental and computational analysis, J. Colloid Interf. Sci. 357 (2011) 243–251, https://doi.org/10.1016/j. icis.2011.01.085.
- [94] S.L. Florez, A.L. Campaña, M.J. Noguera, V. Quezada, O.P. Fuentes, J.C. Cruz, J. F. Osma, CFD analysis and life cycle assessment of continuous synthesis of magnetite nanoparticles using 2D and 3D micromixers, Micromachines 13 (2022) 970, https://doi.org/10.3390/mil3060970.
- [95] E. Chiesa, M. Bellotti, A. Caimi, B. Conti, R. Dorati, M. Conti, I. Genta, F. Auricchio, Development and optimization of microfluidic assisted manufacturing process to produce PLGA nanoparticles, Int. J. Pharm. 629 (2022) 122368, https://doi.org/10.1016/j.ijpharm.2022.122368.
- [96] I.O. De Solorzano, L. Uson, A. Larrea, M. Miana, V. Sebastian, M. Arruebo, Continuous synthesis of drug-loaded nanoparticles using microchannel emulsification and numerical modeling: effect of passive mixing, Int. J. Nanomed. 11 (2016) 3397–3416, https://doi.org/10.2147/IJN.S108812.
- [97] Y. Li, Applications of CFD simulations on microfluidic systems for applications of CFD simulations on microfluidic systems for nanoparticle synthesis nanoparticle synthesis APPLICATIONS OF CFD SIMULATIONS ON MICROFLUIDIC SYSTEMS FOR NANOPARTICLE SYNTHESIS, n.d. https://digitalcommons.lsu.edu/grad school theses
- [98] Z. Xu, H. Liu, A.J. Valocchi, Lattice Boltzmann simulation of immiscible twophase flow with capillary valve effect in porous media, Water Resour. Res. 53 (2017) 3770–3790, https://doi.org/10.1002/2017WR020373.
- [99] L. Scarbolo, D. Molin, P. Perlekar, M. Sbragaglia, A. Soldati, F. Toschi, Unified framework for a side-by-side comparison of different multicomponent algorithms: lattice Boltzmann vs. phasefield model, J. Comput. Phys. 234 (2013) 263–279, https://doi.org/10.1016/j.jcp.2012.09.029.
- [100] M. Dianat, M. Skarysz, A. Garmory, A coupled level set and volume of fluid method for automotive exterior water management applications, Int. J. Multiphase Flow 91 (2017) 19–38, https://doi.org/10.1016/j. ijmultiphaseflow.2017.01.008.
- [101] H. Lee, Water wave generation with source function in the level set finite element framework, J. Mech. Sci. Technol. 29 (2015) 3699–3706, https://doi.org/ 10.1007/s12206-015-0815-5.
- [102] S. Van Der Graaf, T. Nisisako, C.G.P.H. Schroën, R.G.M. Van Der Sman, R. M. Boom, Lattice Boltzmann simulations of droplet formation in a T-shaped

- microchannel, Langmuir 22 (2006) 4144–4152, https://doi.org/10.1021/
- [103] G. Gkogkos, M.O. Besenhard, L. Storozhuk, N.T. Kim Thanh, A. Gavriilidis, Fouling-proof triple stream 3D flow focusing based reactor: design and demonstration for iron oxide nanoparticle co-precipitation synthesis, Chem. Eng. Sci. 251 (2022), https://doi.org/10.1016/j.ces.2022.117481.
- [104] F. Lince, D.L. Marchisio, A.A. Barresi, A comparative study for nanoparticle production with passive mixers via solvent-displacement: use of CFD models for optimization and design, Chem. Eng. Process.: Process Intensif. 50 (2011) 356–368, https://doi.org/10.1016/j.cep.2011.02.015.
- [105] C. Casado, B. Pinho, J. Marugán, L. Torrente-Murciano, Predicting the size of silver nanoparticles synthesised in flow reactors: coupling population balance models with fluid dynamic simulations, Chem. Eng. J. 479 (2024), https://doi. org/10.1016/i.cei.2023.147684.
- [106] M. Shiea, A. Buffo, M. Vanni, D. Marchisio, 183 On: mon, 246 (2025) 13. htt ps://doi.org/10.1146/annurev-chembioeng.
- [107] H. Liu, J. Li, D. Sun, T. Odoom-Wubah, J. Huang, Q. Li, Modeling of silver nanoparticle formation in a microreactor: reaction kinetics coupled with population balance model and fluid dynamics, Ind. Eng. Chem. Res. 53 (2014) 4263–4270, https://doi.org/10.1021/ie4031314.
- [108] H. Liu, H. Zhang, J. Wang, J. Wei, Y. Zhang, Biological synthesis of Pt nanoparticles in a microfluidic chip and modeling of the formation process with PBM and CFD, J. Chem. Technol. Biotechnol. 92 (2017) 2171–2177, https://doi. org/10.1002/jctb.5233.
- [109] S. Shin, C. Devos, A.P. Udepurkar, P.K. Inguva, A.S. Myerson, R.D. Braatz, Mechanistic modeling of lipid nanoparticle (LNP) precipitation via population balance equations (PBEs), (2025). http://arxiv.org/abs/2504.10533.
- [110] H. Liu, H. Zhang, J. Wang, J. Wei, Y. Zhang, Biological synthesis of Pt nanoparticles in a microfluidic chip and modeling of the formation process with PBM and CFD, J. Chem. Technol. Biotechnol. 92 (2017) 2171–2177, https://doi. org/10.1002/jctb.5233
- [111] P. Valeh-e-Sheyda, E. Mir, Nucleation rate prediction of curcumin particles in microfluidic-assisted nanoprecipitation, Chem. Eng. Technol. 44 (2021) 174–182, https://doi.org/10.1002/ceat.202000360.
- [112] T. Jaouhari, F. Zhang, T. Tassaing, S. Fery-Forgues, C. Aymonier, S. Marre, A. Erriguible, Process intensification for the synthesis of ultra-small organic nanoparticles with supercritical CO2 in a microfluidic system, Chem. Eng. J. 397 (2020). https://doi.org/10.1016/j.cgi.2020.125333.
- [113] Y. Karimi, A.R. Solaimany Nazar, M. Motevasel, CFD simulation of nanofluid heat transfer considering the aggregation of nanoparticles in population balance model, J. Therm. Anal. Calorim. 143 (2021) 671–684, https://doi.org/10.1007/ s10973-019-09218-0.
- [114] S.L. Florez, A.L. Campaña, M.J. Noguera, V. Quezada, O.P. Fuentes, J.C. Cruz, J. F. Osma, CFD analysis and life cycle assessment of continuous synthesis of magnetite nanoparticles using 2D and 3D micromixers, Micromachines 13 (2022), https://doi.org/10.3390/mil3060970.
- [115] A.B. de Almeida, E. Fontana, A.V.L. Machado, L.F.L. Luz, Application of CFD in nanoremediation problems with nanoscale zero-valent iron particles, Chem. Eng. Trans. 98 (2023) 219–224. https://doi.org/10.3303/CFT2398037
- Trans. 98 (2023) 219–224, https://doi.org/10.3303/CET2398037.

 [116] F. Bally, D.K. Garg, C.A. Serra, Y. Hoarau, N. Anton, C. Brochon, D. Parida, T. Vandamme, G. Hadziioannou, Improved size-tunable preparation of polymeric nanoparticles by microfluidic nanoprecipitation, Polymer 53 (2012) 5045–5051, https://doi.org/10.1016/j.polymer.2012.08.039
- https://doi.org/10.1016/j.polymer.2012.08.039.

 [117] H. Liu, J. Huang, D. Sun, L. Lin, W. Lin, J. Li, X. Jiang, W. Wu, Q. Li, Microfluidic biosynthesis of silver nanoparticles: effect of process parameters on size distribution, Chem. Eng. J. 209 (2012) 568–576, https://doi.org/10.1016/j.
- [118] L. Capretto, W. Cheng, D. Carugo, O.L. Katsamenis, M. Hill, X. Zhang, Mechanism of co-nanoprecipitation of organic actives and block copolymers in a microfluidic environment, Nanotechnology 23 (2012), https://doi.org/10.1088/0957-4484/ 23/37/375602.
- [119] G.T. Vladisavljević, A. Laouini, C. Charcosset, H. Fessi, H.C.H. Bandulasena, R. G. Holdich, Production of liposomes using microengineered membrane and coflow microfluidic device, Colloids Surf. A Physicochem. Eng. Asp. 458 (2014) 168–177. https://doi.org/10.1016/j.colsurfa.2014.03.016.
- 168–177, https://doi.org/10.1016/j.colsurfa.2014.03.016.
 [120] A.G. Olenskyj, Y. Feng, Y. Lee, Continuous microfluidic production of zein nanoparticles and correlation of particle size with physical parameters determined using CFD simulation, J. Food Eng. 211 (2017) 50–59, https://doi.org/10.1016/j.jfoodeng.2017.04.019.
- [121] M. Rahimi, P. Valeh-e-Sheyda, R. Zarghami, H. Rashidi, On the mixing characteristics of a poorly water soluble drug through microfluidic-assisted nanoprecipitation: experimental and numerical study, Can. J. Chem. Eng. 96 (2018) 1098–1108, https://doi.org/10.1002/cjce.23074.
- [122] O. Kašpar, A.H. Koyuncu, A. Pittermannová, P. Ulbrich, V. Tokárová, Governing factors for preparation of silver nanoparticles using droplet-based microfluidic

- device, Biomed. Microdev. 21 (2019), https://doi.org/10.1007/s10544-019-0435-4
- [123] S. Soheili, E. Mandegar, F. Moradikhah, M. Doosti-Telgerd, H.A. Javar, Experimental and numerical studies on microfluidic preparation and engineering of chitosan nanoparticles, J. Drug Deliv. Sci. Technol. 61 (2021), https://doi.org/ 10.1016/j.jddst.2020.102268.
- [124] B. Benyahia, M.V. Bandulasena, H.C.H. Bandulasena, G.T. Vladisavljević, Experimental and computational analysis of mixing inside droplets for microfluidic fabrication of gold nanoparticles, Ind. Eng. Chem. Res. 60 (2021) 13967–13978, https://doi.org/10.1021/acs.iecr.1c01960.
- [125] N. Kimura, M. Maeki, K. Sasaki, Y. Sato, A. Ishida, H. Tani, H. Harashima, M. Tokeshi, Three-dimensional, symmetrically assembled microfluidic device for lipid nanoparticle production, RSC Adv. 11 (2021) 1430–1439, https://doi.org/ 10.1039/d0ra08826a.
- [126] M. Akbari, Z. Rahimi, M. Rahimi, Chitosan/tripolyphosphate nanoparticles in active and passive microchannels, Res. Pharm. Sci. 16 (2021) 79–93, https://doi. org/10.4103/1735-5362.305191.
- [127] O. Sartipzadeh, S.M. Naghib, F. Haghiralsadat, F. Shokati, M. Rahmanian, Microfluidic-assisted synthesis and modeling of stimuli-responsive monodispersed chitosan microgels for drug delivery applications, Sci. Rep. 12 (2022), https:// doi.org/10.1038/s41598-022-12031-9.
- [128] Y. Kim, B.L. Chung, M. Ma, W.J.M. Mulder, Z.A. Fayad, O.C. Farokhzad, R. Langer, Mass production and size control of lipid-polymer hybrid nanoparticles through controlled microvortices, Nano Lett. 12 (2012) 3587–3591, https://doi. org/10.1001/j.1301.253v
- [129] S.G. Bariki, S. Movahedirad, M. Ghojavand, <scp>CFD</scp>study of polycaprolactone nanoparticles precipitation in a co-flow capillary micro-tube, Can. J. Chem. Eng. (2022), https://doi.org/10.1002/cjce.24768.
- [130] M. Ježková, P. Jelínek, O. Marelja, D. Trunov, M. Jarošová, Z. Slouka, M. Šoóš, The preparation of mono- and multicomponent nanoparticle aggregates with layer-by-layer structure using emulsion templating method in microfluidics, Chem. Eng. Sci. 247 (2022), https://doi.org/10.1016/j.ces.2021.117084.
- [131] P. Pico, K. Nathanael, A.D. Lavino, N.M. Kovalchuk, M.J.H. Simmons, O.K. Matar, Silver nanoparticles synthesis in microfluidic and well-mixed reactors: a combined experimental and PBM-CFD study, Chem. Eng. J. 474 (2023), https://doi.org/10.1016/j.cej.2023.145692.
- [132] F. Raji, M. Kazemeini, Effects of the microchannel shape upon droplet formations during synthesis of nanoparticles, n.d.
- [133] J.F. Wilson, M. Kroupa, J. Kosek, M. Soos, Numerical study of soft colloidal nanoparticles interaction in shear flow, Langmuir 34 (2018) 15600–15611, https://doi.org/10.1021/acs.langmuir.8b03350.
- [134] S.G. Sontti, A. Atta, Numerical insights on controlled droplet formation in a microfluidic flow-focusing device, Ind. Eng. Chem. Res. 59 (2020) 3702–3716, https://doi.org/10.1021/acs.iecr.9b02137.
- [135] I.L. Chaves, L.C. Duarte, W.K.T. Coltro, D.A. Santos, Droplet length and generation rate investigation inside microfluidic devices by means of CFD simulations and experiments, Chem. Eng. Res. Des. 161 (2020) 260–270, https:// doi.org/10.1016/j.cherd.2020.07.015.
- [136] L. Shang, Y. Cheng, Y. Zhao, Emerging droplet microfluidics, Chem. Rev. 117 (2017) 7964–8040, https://doi.org/10.1021/acs.chemrev.6b00848.
- [137] T. Glawdel, C. Elbuken, C.L. Ren, Droplet generation in microfluidics. Encyclopedia of Microfluidics and Nanofluidics, Springer US, 2013, pp. 1–12, https://doi.org/10.1007/978-3-642-27758-0_1713-1.
- [138] L. Bai, Y. Fu, S. Zhao, Y. Cheng, Droplet formation in a microfluidic T-junction involving highly viscous fluid systems, Chem. Eng. Sci. 145 (2016) 141–148, https://doi.org/10.1016/j.ces.2016.02.013.
- [139] E. Roumpea, N.M. Kovalchuk, M. Chinaud, E. Nowak, M.J.H. Simmons, P. Angeli, Experimental studies on droplet formation in a flow-focusing microchannel in the presence of surfactants, Chem. Eng. Sci. 195 (2019) 507–518, https://doi.org/ 10.1016/j.ces.2018.09.049.
- [140] Q.Q. Xiong, Z. Chen, S.W. Li, Y.D. Wang, J.H. Xu, Micro-PIV measurement and CFD simulation of flow field and swirling strength during droplet formation process in a coaxial microchannel, Chem. Eng. Sci. 185 (2018) 157–167, https://doi.org/10.1016/j.ces.2018.04.022.
- [141] F. Shen, Y. Li, Z. Liu, X.J. Li, Study of flow behaviors of droplet merging and splitting in microchannels using Micro-PIV measurement, Microfluid. Nanofluid. 21 (2017), https://doi.org/10.1007/s10404-017-1902-y.
- [142] C. Brücker, C. Brücker, Volumetric PIV view project nature inspired flow sensing and manipulation view project PIV in two-phase flows, n.d. https://www. researchgate.net/publication/234082457.
- [143] W. Lan, S. Li, Y. Wang, G. Luo, CFD simulation of droplet formation in microchannels by a modified level set method, Ind. Eng. Chem. Res. 53 (2014) 4913–4921, https://doi.org/10.1021/ie403060w.